A&A, 709, A97 (2026)
https://doi.org/10.1051/0004-6361/202659021

Astronomy & Astrophysics

OB runaway stars originating in the Vel OB1 association

N. Azatyan[1,⋆], L. Kaper[2], A. Samsonyan[1], M. Stoop[2], D. Andreasyan[1], J. van den Eijnden[2], and E. Nikoghosyan[1]

[1] Byurakan Astrophysical Observatory, 0213, Aragatsotn prov., Armenia
[2] Anton Pannekoek Institute for Astronomy, University of Amsterdam, Science Park 904, 1098 XH Amsterdam, The Netherlands

Received 18 January 2026 / Accepted 7 April 2026

ABSTRACT

Context. OB runaway stars are massive stars moving through interstellar space with a high velocity (up to 200 km s^{-1}). They are produced by dynamical ejections in young massive clusters or by supernova explosions in massive binaries. OB runaways can travel several hundred parsec before exploding as supernovae, affecting the dynamical and chemical evolution of the Galaxy.
Aims. The Vel OB1 association is one of the largest OB associations, hosting about 20 O-type and more than 50 B-type stars. Our aim is to find OB runaway stars in this region. By quantifying their number and identifying their parent clusters, we seek to better understand their production channels and their impact on the surrounding medium.
Methods. We used *Gaia* DR3 coordinates, parallaxes, and proper motions of massive stars in the field centred on Vel OB1 to identify OB runaways by measuring their peculiar velocity. Under suitable physical conditions, OB runaways create observable bow shocks in the interstellar medium (ISM). We inspected infrared WISE images to identify wind bow shocks and their associated OB runaways. By reconstructing their path, we tried to locate their parent cluster and estimate their travel times.
Results. We identified six young stellar clusters hosting most of the massive-star population in Vel OB1 (distance 1.6−2.1 kpc; age 1−10 Myr). From the tangential velocity distribution of the members, we derived a threshold velocity of 15 km s^{-1} to classify a star as a runaway. We identified 25 OB runaways (including the high-mass X-ray binary Vela X-1) and one F-type runaway. We detected 16 arc-like features, four for the first time, and six of the features are associated with OB runaways selected by peculiar velocity. Ten bow shocks are aligned with the proper motion of the runaways. Parent clusters are identified for seven runaways. Most likely, the majority of these runaways are produced by dynamical ejection.
Conclusions. The runaway fraction of the young stellar population in Vel OB1 is about 30%. Many OB runaways, even some far above the Galactic plane, produce wind bow shocks, which consequently reveal information on local ISM conditions.

Key words. binaries: general – stars: early-type – stars: mass-loss – open clusters and associations: individual: VelOB1 – X-rays: binaries

1. Introduction

Massive stars in the Milky Way are predominantly found in organised stellar groupings rather than being uniformly distributed across the Galactic disc. Observational surveys have indicated that roughly 80% of O-type stars reside in clusters or associations associated with spiral arms (Brown et al. 1999). The remaining population displays kinematic properties that are inconsistent with in situ formation, implying that these stars originated in clustered environments but were subsequently ejected; such objects are commonly referred to as runaway stars (Blaauw 1993; de Wit et al. 2005; Gvaramadze et al. 2012). Two main physical mechanisms have been proposed to account for the origin of OB runaways and their large peculiar velocities. In one channel, close gravitational encounters in young, dense clusters dynamically expel massive stars at high velocities (Poveda et al. 1967; Gvaramadze 2009; Fujii & Portegies Zwart 2011; Stoop et al. 2024a). In the other, a supernova explosion in a massive binary system disrupts the orbit and accelerates the surviving companion (Blaauw 1961; van Rensbergen et al. 1996; Kaper et al. 1997). In this supernova-driven scenario, which assumes symmetric mass loss during the explosion, the ejection velocity of the secondary is set by its pre-explosion orbital motion. The binary remains gravitationally bound only if the fraction of mass removed is less than half of the total system mass (Blaauw 1961; Boersma 1961).

A growing body of observational and theoretical work suggests that both mechanisms operate in nature (Gies 1987; Hoogerwerf et al. 2000; Kaper 2000; Gualandris et al. 2004; Boubert et al. 2017), although their relative importance remains uncertain. In addition, combined pathways have been proposed in which a massive binary is first ejected from its natal cluster through dynamical interactions and subsequently experiences an additional velocity boost following a supernova explosion of one component (Pflamm-Altenburg & Kroupa 2010; Gvaramadze et al. 2018; Dorigo Jones et al. 2020). In turn, the study of OB runaways provides insight into the physical conditions of young massive clusters.

The velocity threshold historically adopted to define O- and B-type runaway stars is ∼30 km s^{-1}, as the typical (radial) velocity of massive stars is of the order of 10 km s^{-1} with respect to the local standard of rest (LSR), as was the accuracy of these measurements back then (e.g. Blaauw 1961; Hoogerwerf et al. 2000; de Wit et al. 2005; Eldridge et al. 2011; Boubert & Evans 2018). More recent binary evolution models predict that a significant fraction of ejected systems acquire substantially lower velocities, leading to the introduction of the term 'walkaway stars' for these objects (Renzo et al. 2019). But there is no physical reason why

⋆ Corresponding author: nayazatyan@bao.sci.am

a threshold velocity of 30 km s^{-1} has been introduced, and the escape velocity of the parent cluster (a few km s^{-1}) may be more appropriate.

In addition to their anomalously large space velocities, massive runaway stars are often characterised by the presence of wind-driven bow shocks (e.g. van Buren & McCray 1988; Gvaramadze & Bomans 2008; Peri et al. 2012; Mackey 2023). These bow shocks typically extend over parsec scales and emit strongly at infrared wavelengths, which makes them observable over large distances despite the effects of interstellar extinction (e.g. Gvaramadze et al. 2010, 2011). While early studies focused primarily on their mid-infrared signatures, subsequent observations have revealed that bow shocks associated with runaway stars can also be detected across a broader range of wavelengths, including optical and radio bands (Kaper et al. 1997; Gvaramadze & Bomans 2008; Gvaramadze et al. 2014; Benaglia et al. 2010; van den Eijnden et al. 2022; Moutzouri et al. 2025).

OB runaway stars provide a valuable means of tracing the properties of the surrounding interstellar medium (ISM), as their strong stellar winds interact directly with the ambient gas during their motion. When a runaway star travels at supersonic velocity relative to the local medium, the momentum flux of the stellar wind can balance the external ram pressure, leading to the formation of a wind-driven bow shock (Baranov et al. 1971; Comeron & Kaper 1998). Observational searches have revealed such structures around a fraction of OB runaways, with van Buren et al. (1995) reporting a detection rate of roughly 30%. The absence of detectable bow shocks in many cases can be attributed to variations in ISM conditions. For instance, a high sound speed in the surrounding gas may prevent the development of a supersonic flow, or a low ambient density may reduce the observability of the interaction (Huthoff & Kaper 2002). Moreover, the alignment of the bow shock with the (peculiar) velocity of the runaway depends on the relative velocity of the system with respect to the ISM (Bodensteiner et al. 2018).

OB runaways provide important information on the dynamical evolution of stellar clusters (dynamical ejection scenario), and on binary evolution (supernova scenario). A key step in such analyses is the identification of the parent cluster or association, as this enables an estimate of the kinematic age of the runaway. When this timescale is comparable to the age of the host cluster, a dynamical ejection origin is favoured. Conversely, a substantially shorter kinematic age points towards a supernova-related ejection from a massive binary. In this case, the cluster age at the moment of ejection constrains the initial mass of the progenitor that underwent core collapse, while the present-day velocity of the runaway provides information on the amount of mass ejected during the explosion (Ankay et al. 2001; van der Meij et al. 2021). As a natural consequence of the supernova channel, high-mass X-ray binaries (HMXBs) – systems composed of a massive donor star and a compact remnant – are expected to exhibit runaway characteristics (van den Heuvel et al. 2000). Carretero-Castrillo et al. (2023) confirmed seven HMXBs as runaways out of a sample of 152 systems (Fortin et al. 2023). This sample includes both OB-supergiant systems (52) and Be/X-ray binaries (74). When interpreting these results, one needs to take into account that van den Heuvel et al. (2000) propose that OB-supergiant systems get a substantially higher space velocity (about 50 km s^{-1}) than the lower-mass Be/X-ray binaries (about 15 km s^{-1}). Furthermore, Renzo et al. (2019) predict systematically lower space velocities for these systems. Thus, the value of the threshold velocity above which systems are identified as runaway candidates is also important. In systems hosting a black hole, such as Cyg X-1, the mass lost during the supernova event is expected to be small, potentially resulting in negligible recoil velocities (Mirabel & Rodrigues 2003; Rao et al. 2020).

On larger scales, the ejection of massive stars from their natal environments has important implications for star cluster evolution and Galactic ecology. Numerical studies have indicated that up to 20–30% of the most massive stars formed in clusters may escape within a few million years (Stoop et al. 2024a), an effect that must be accounted for when constraining the high-mass end of the initial mass function. Also, massive stars have a dominant impact on their surrounding medium (UV radiation, stellar wind, supernova explosion). As OB runaway stars may travel several tens to hundreds of parsec away from their birth place, they reach locations where the ISM is much more tenuous than inside the dense molecular clouds confined to the Galactic plane. Therefore, the study of OB runaways is of key importance to our understanding of the dynamical and chemical evolution of the Galaxy (Andersson et al. 2020).

The astrometric and photometric data provided by the *Gaia* mission make it possible to search for runaways in order to determine membership and the age of their potential parent clusters, and to reconstruct the kinematic and evolutionary history of these systems. The target of our study is the Vel OB1 association. Vel OB1, at a distance of 1.6–2.5 kpc, is one of the largest OB associations known (Humphreys 1978; Bassino et al. 1982; Sahu 1992). Humphreys (1978) derived an angular extent of Vel OB1 (l = 262° to 268°, b = −2.7° to +1.4°) and identified 17 probable members. Later, Reed (2000) expanded the size of the association (l = 255° to 275°, b = −5° to +5°)[1] and extended the list of candidate members of Vel OB1 to 70 stars, including HD 77581, the B supergiant companion to the X-ray pulsar Vela X-1. Fig. 1 shows the region on the sky including Vel OB1. In the foreground several other star-forming regions and stellar clusters are present, such as Vel OB2 (not included in Fig. 1) at a distance of 410 pc (Armstrong et al. 2022) and RCW36 at a distance of 700 pc (Ellerbroek et al. 2013). Table A.1 lists the proposed members of Vel OB1 collected from the literature. The table lists the location, spectral type, and radial velocity (V_r) of these candidate members. We include the *Gaia* DR3 parallax, proper motion, and G-band magnitude for these stars. The mean radial velocity of Vel OB1 is 23 ± 4 km s^{-1}, and the median proper motion along the Galactic longitude and latitude are −6.78 ± 1.07 mas yr^{-1} and −1.69 ± 0.25 mas yr^{-1}, respectively (see also Mel'nik & Dambis 2017).

Star formation in Vel OB1 has been continuous between 4 and 20 Myrs ago (van Rensbergen et al. 1996). The region contains several young stellar clusters, such as RCW34, RCW38, and RCW41 (Figs. 1, A.1, Table 1). The top-left panel in Fig. A.2 displays the *Gaia* DR3 distance distribution of the candidate members of Vel OB1 according to Humphreys (1978) (orange) and Reed (2000) (blue). This provides a rough estimate of the distance range of Vel OB1. In the lower panel of Fig. A.2 we plot the proper motion of the candidate members (Table A.1, Humphreys 1978; Reed 2000) of the Vel OB1 association (circles). Thus, the main fraction of the candidate members is concentrated in the range μ_{l^*} = (−8.6;−4.9) mas yr^{-1} and μ_b = (−3.1;0.5) mas yr^{-1}. This information serves as an additional aid in reducing the *Gaia* DR3 sample (Section 2.1) and the identification of other members of the Vel OB1 association.

The aim of this paper is to search for OB runaways in the region contained by the OB association Vel OB1. We have organised the paper as follows: Section 2 presents the membership

[1] This roughly corresponds to a range in RA from 08h12 to 09h24 and in Dec from −36° to −53°.

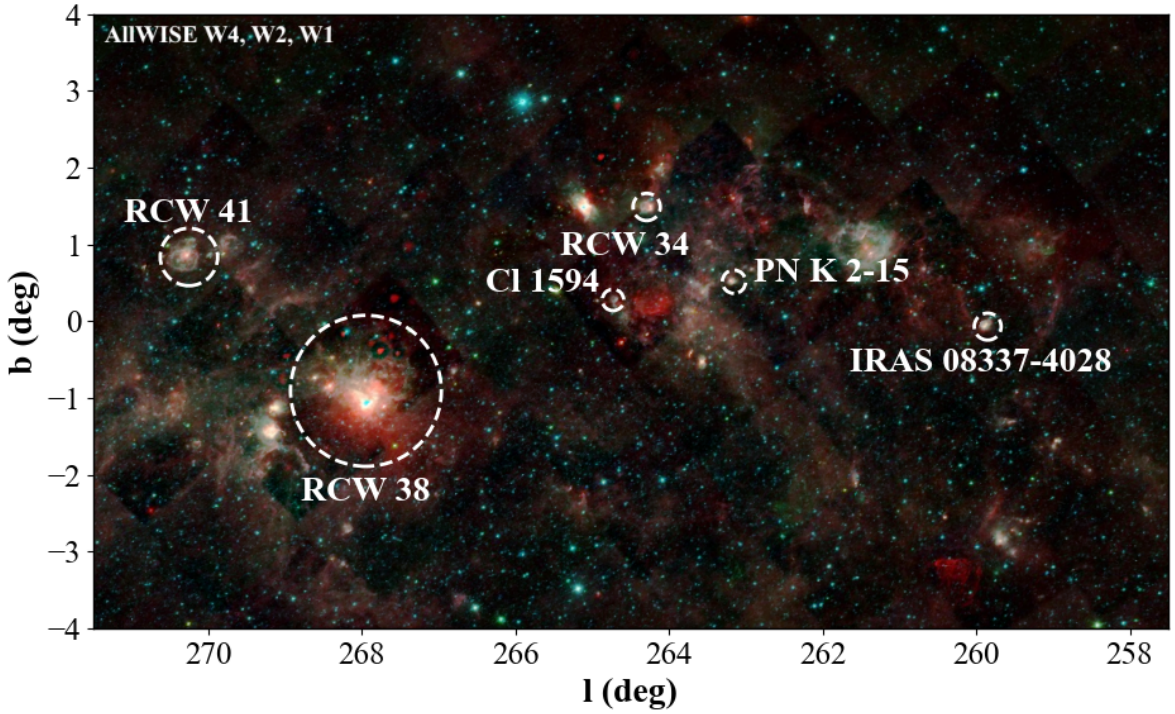

Fig. 1. Vel OB1 association: the extension on the sky according to the limits proposed by Reed (2000). Indicated are several young stellar clusters embedded in this region, within the distance interval of about 1.6 to 2.5 kpc. Some star-forming regions and clusters (not labelled) are in the foreground to Vel OB1, e.g. Vel OB2 (just below the plotted region at 410 pc) and RCW 36 (l = 265.1, b = 1.4, at a distance of 700 pc). The background image is a colour composite of the AllWISE survey in bands W1, W2, and W4. Milky Way Star Cluster Nº 1594 ([KPS2012] MWSC 1594, Kharchenko et al. 2013) is indicated as Cl 1594.

Table 1. Young stellar clusters in Vel OB1.

Name	l	b	N	Parallax	μ_{l^*}	μ_b	V_{LSR}	D	Age	A_V	p
–	(deg)	(deg)	–	(mas)	(mas yr^{-1})	(mas yr^{-1})	(km s^{-1})	(pc)	(Myr)	(mag)	–
(1)	(2)	(3)	(4)	(5)	(6)	(7)	(8)	(9)	(10)	(11)	(12)
Cl 1594	264.73	0.27	21	0.480±0.010	−6.498±0.452	−1.203±0.589	6.8±3.9	$2084^{+43.0}_{-41.3}$	2.6–6.6	5	–
IRAS 08337-4028	259.95	0.02	14	0.624±0.012	−5.979±0.833	−2.108±0.982	10.8±5.2	$1603^{+31.7}_{-30.5}$	5.0–8.9	5	–
PN K 2-15	263.24	0.52	12	0.560±0.007	−7.125±0.402	−1.074±0.533	8.3±2.9	$1787^{+23.0}_{-22.4}$	0.5–3.0	5	–
RCW 34	264.35	1.44	48	0.509±0.005	−6.773±0.487	−0.826±0.763	8.2±4.6	$1967^{+18.4}_{-18.0}$	4.7–9.9	4	0.85
RCW 38	267.94	−1.06	378	0.560±0.001	−6.682±0.359	−1.052±0.346	4.3±3.6	$1785^{+4.2}_{-4.1}$	3.2–7.1	3	0.9
RCW 41	270.24	0.83	35	0.645±0.006	−6.682±0.367	−0.913±0.370	4.5±2.3	$1550^{+14.6}_{-14.3}$	0.7–1.0	7	0.7

Notes. (1) Name of the region, (2), (3) Galactic coordinates, (4) number of members based on the membership probability p, (5) *Gaia* DR3 parallaxes with 1σ uncertainties, (6–7) mean proper motion with their standard deviation, (8) tangential velocity of the cluster with respect to the LSR with 1σ uncertainty, (9) distance from *Gaia* DR3 parallax with 1σ uncertainties, (10) and (11) the age range based on 100 iterations and a fixed extinction, respectively, and (12) the membership probability. The [KPS2012] MWSC 1594 open cluster is indicated as Cl 1594.

analysis of six young clusters in Vel OB1 based on *Gaia* DR3 data and OB stars listed as members of Vel OB1 in Reed (2000). We used these young clusters as a representation of the young stellar population of Vel OB1 and searched for OB runaways potentially originating in and moving with high velocity with respect to these clusters. In Section 3 we describe our search for OB runaways in Vel OB1, either based on their peculiar velocity and/or the presence of a wind bow shock. We also summarise their properties. In Section 4 we identify the parent cluster of a small subset of the OB runaways. In Section 5 we analyse the detected arc-like features and investigate whether the stellar wind and ambient medium parameters are consistent with the interpretation that these features are due to a wind bow shock. In Section 6 we compare our results with earlier work, discuss the possible scenarios producing these OB runaways, and determine the conditions of the ISM in case a wind bow shock has been detected. In Section 7 we summarise our conclusions.

2. Young stellar clusters in Vel OB1

In this section, we describe the procedure for selecting stars from the *Gaia* DR3 database in order to identify members of the Vel OB1 association and the stellar clusters located within this region. Our analysis reveals seventeen stellar overdensities, six of which are young stellar clusters that constitute the main components of Vel OB1. In the following, we focus on the search for

OB runaway stars originating from Vel OB1, and in particular from these young clusters.

2.1. Gaia DR3 analysis

Based on the historical definition of Vel OB1, we queried the *Gaia* database (DR3; Gaia Collaboration 2022) in the range of Galactic longitude $l = 255°$ to $275°$, and Galactic latitude $b = -5°$ to $+5°$. The initial dataset includes ∼15 million sources. We corrected the parallax taking into account the zero-point offset estimated from quasars (Lindegren et al. 2021).

The initial sample was refined using a series of astrometric quality criteria. First, we excluded sources with a Renormalised Unit Weight Error (`ruwe`) exceeding 1.4, which typically signals unreliable astrometric solutions and is often associated with unresolved multiplicity. Second, we removed objects with fewer than ten visibility periods contributing to the astrometric fit (`visibility_periods_used` < 10), as such cases may suffer from systematic astrometric or photometric effects (Gaia Collaboration 2021). Third, sources with an image parameter determination goodness-of-fit harmonic amplitude (`ipd_gof_harmonic_amplitude`) larger than 0.15 were discarded, since elevated values are indicative of crowding or binarity (Gaia Collaboration 2021). In addition, we excluded stars for which multiple peaks were detected in the image parameter determination (`ipd_frac_multi_peak`), as well as sources flagged as duplicated (`duplicated_source`), both of which point to potentially problematic astrometric solutions. Finally, we required the parallax to be measured with sufficient precision by retaining only sources with a fractional parallax uncertainty more than 5 (`parallax/parallax_error` > 5).

The remaining sample consists of approximately two million sources. The next step is to search for stellar over-densities in Galactic longitude, Galactic latitude, parallax and proper motion using the Tool for OPerations on Catalogues And Tables (TOPCAT; Pössel 2020), until we obtain samples that correspond to stellar clusters included in the Vel OB1 association, and field stars. The result of that selection is shown in Fig. A.1 where we present the parallax distribution as a function of Galactic longitude and the distribution of stellar over-densities in Galactic coordinates, respectively. The parallax distribution indicates an excess of stars in the range from about 0.40 mas to 0.65 mas, which coincides well with the distance of the candidate members of the Vel OB1 association. The position and putative size of the young stellar clusters are shown (see Sect. 2.2 below for a membership analysis).

2.2. Membership analysis young stellar clusters

We carefully inspected the stellar over-densities in the region contained by Vel OB1 (in the parallax range 0.40–0.65 mas). Apart from six young stellar clusters (Table 1), we identified 11 stellar clusters corresponding to open clusters listed in the *Simbad* astronomical database.

Cluster membership was determined using the PYUPMASK package, a PYTHON-based implementation of the unsupervised clustering algorithm UPMASK (Krone-Martins & Moitinho 2014; Pera et al. 2021). The analysis was performed in a five-dimensional astrometric parameter space defined by sky position, parallax, and proper motion. Radial velocities were intentionally excluded, as they are available for only a subset of sources in *Gaia* DR3 (Katz et al. 2023); including them would introduce systematic differences between stars with and without measured radial velocities. The algorithm proceeds through a two-level iterative scheme. In the internal clustering step, groups of approximately 25 stars are identified using a Gaussian mixture model, which has been shown to provide optimal performance for this method (Pera et al. 2021). In the subsequent resampling stage, observational uncertainties are incorporated by repeatedly drawing astrometric parameters from their Gaussian error distributions, while correlations between parameters and between stars are neglected. We performed 10 000 resampling iterations and employed a Gaussian–uniform mixture model to reduce contamination by spurious members. The PYUPMASK analysis was restricted to regions containing more than 25 sources (i.e. the RCW clusters), whereas membership in sparser regions was assessed manually.

For each star, a membership probability p was assigned based on the fraction of iterations in which it was classified as a cluster member. The threshold value of p used to distinguish members from field stars was not fixed globally, but instead selected individually for each region after inspecting the noise characteristics of the resulting probability distribution.

Table 1 lists the parameters of the young stellar clusters in Vel OB1 based on the membership analysis. The zoomed area in the top-right panel of Fig. A.2 shows the proper motion distribution of the members of these clusters. As can be seen, their proper motions are in the same range as the main fraction of the candidate members of Vel OB1 (Table A.1).

2.2.1. Membership and distance of the young clusters

We analysed the parallax distribution of the members of each cluster against their G-magnitude (the individual panels are included in Appendix A, Fig. B.1). We determined the distance to each cluster through a log-likelihood function as in Stoop et al. (2024b). For an assumed distance, we computed the likelihood of the observed parallaxes using Gaussian uncertainties without explicitly normalising the probability distribution. The most probable distance corresponds to the maximum of the resulting log-likelihood function, while the associated 1σ confidence interval was derived from the 16th and 84th percentiles of the distance distribution implied by the likelihood. The determined best-fit parallax, distance and their 1σ uncertainties are in the range 1.6–2.1 kpc (Table 1), with RCW 38 the richest young cluster at 1.8 kpc. The sky distribution of the cluster members can be found in Appendix A (Fig. B.2).

If we take the six young clusters to define the current distance and motion of Vel OB1, it is located at a distance of 1.85 kpc with a mean proper motion $\mu_l^* = -6.76 \pm 0.49$ mas yr^{-1} and $\mu_b = -1.03 \pm 0.53$ mas yr^{-1}, which is in good agreement with the proper motion $\mu_l^* = -6.78 \pm 1.07$ mas yr^{-1} and $\mu_b = -1.09 \pm 0.25$ mas yr^{-1} reported in Mel'nik & Dambis (2017) (Fig. A.2). The mean radial velocity of Vel OB1 is 25 ± 15 km s^{-1} (based on the members of Vel OB1 with a measured radial velocity), which is also in good correspondence with the mean radial velocity of 23 ± 4 km s^{-1} reported in Mel'nik & Dambis (2017). The peculiar velocity of Vel OB1 with respect to its LSR is 9.6 ± 3.9 km s^{-1}; for more details we refer to Sect. 3.1.

In column (13) of Table A.1 we reassess the membership of Vel OB1 based on the *Gaia* DR3 membership analysis. If the candidate (according to Humphreys 1978 and Reed 2000) is member of one of the young clusters, we list the name of the respective cluster. If the candidate's parallax is in the range between 0.4 and 0.65 marcsec and the proper motion μ_l^* between −8.6 and −4.9 mas yr^{-1} and μ_b between −3.1 and 0.5 mas yr^{-1}, we assign it as a member of Vel OB1 (Y). These limits are based on the observed range in parallax and proper motion of the young clusters (Table 1).

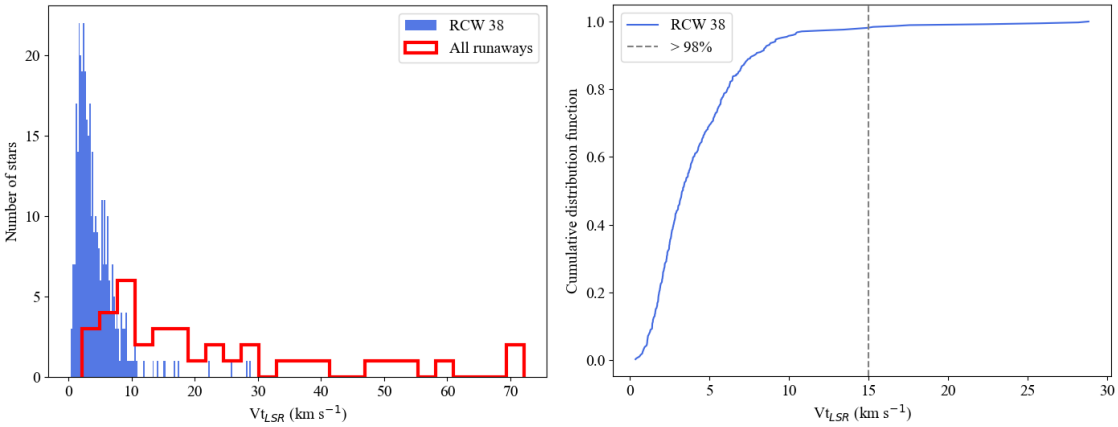

Fig. 2. OB-runaway peculiar tangential velocity threshold. *Left panel*: tangential velocity of the members (blue) of the young cluster RCW38 with respect to the LSR velocity: the peculiar tangential velocity $v^t_{\rm LSR}$. The red histogram shows $v^t_{\rm LSR}$ for all OB runaways identified in this region. *Right panel*: cumulative distribution of $v^t_{\rm LSR}$ for the members of RCW38. We note that 98% of the members have a peculiar tangential velocity less than 15 km s^{-1}. We take this value as the threshold for the tangential peculiar velocity to identify the star as a runaway.

2.2.2. Age of the young clusters

For each young cluster, the colour-absolute magnitude diagram is used to constrain the age (Appendix A, Fig. B.3). To estimate the age of the individual clusters, we generated `PARSEC (v2.0) + COLIBRI (S_37 + S_35 + PR16)` (Padova and Trieste Stellar Evolution Code) isochrones[2] considering an age range from 0.2 Myr to 10 Myr with steps of 0.1 Myr (Bressan et al. 2012; Marigo et al. 2013; Rosenfield et al. 2016; Marigo et al. 2017; Pastorelli et al. 2019, 2020; Nguyen et al. 2022). To identify the best-fit isochrone for our clusters, we used the statistical estimation and likelihood maximisation standard methods described in van der Meij et al. (2021). To estimate the age dispersion for each cluster, we use a bootstrap method. We repeat the age determination 100 times on randomly selected samples, which contain 90% of all cluster members. Columns (10) and (11) of Table 1 list the thus obtained age range based on 100 iterations and a fixed extinction; to estimate the (average) extinction A_V we used the near-infrared counterparts of the members, and their colours (adopting $R_V = 3.1$). The derived ages are in accordance with previous estimates and range from 0.5 to 10 Myr. We defer a more detailed discussion on the young massive clusters included in Vel OB1 to a future paper.

3. OB runaways in Vel OB1

The main aim of this paper is to search for OB runaways in the region contained by the OB association Vel OB1. One way to identify OB runaways is by estimating their peculiar velocity, i.e. by comparing their proper motion (and/or radial velocity) to the LSR velocity, or to the mean velocity of the young clusters contained in Vel OB1 (Sect. 3.1). The former is obtained from a model describing the differential Galactic rotation and by taking into account the peculiar solar motion and the distance (the latter in Sect. 2.2). An alternative approach is to look for the presence of a wind bow shock produced by the supersonic motion of the OB runaway, and the interaction of its stellar wind with the ambient medium (Sect. 3.2).

The peculiar velocity threshold of 30 km s^{-1} is rather arbitrary; in order to escape from a stellar cluster the OB runaway velocity should exceed the escape velocity of the cluster which is of the order of 5−10 km s^{-1} for a young massive cluster; the tangential velocity dispersion in these clusters is in the range 1−2 km s^{-1} (Stoop et al., in prep.). For the formation of a stellar wind bow shock, however, it is sufficient that the stellar velocity exceeds the local sound speed in the ISM, which can be as low as the escape velocity of young clusters. Renzo et al. (2019) introduced the term 'walkaway' to emphasise the point that OB runaways (in this particular case produced by the binary supernova scenario) are also predicted to travel with a space velocity lower than 30 km s^{-1}. In fact, some of the OB runaways for which we observe a wind bow shock have a space velocity consistent with those of massive stars in clusters (see Fig. 2).

3.1. Runaways identified by their peculiar velocity

To investigate the runaway nature of the OB stars in Vel OB1 (Table A.1), we calculate the peculiar velocity $V_{\rm pec}$ of each star relative to the LSR. To achieve this, we first used the Galactocentric transformations of Johnson & Soderblom (1987) to determine the mean Galactocentric velocity (U, V, W) components of nearby stars within 100 pc of each OB star, using the same approach as for the OB stars themselves. Specifically, we subtracted the predicted Galactic rotation velocity at the location of the star (Binney & Merrifield 1998; Binney & Tremaine 2008) from its observed proper motion and radial velocity (if available):

$$V_{\rm pec} = \sqrt{(U_* - U_{\rm sys})^2 + (V_* - V_{\rm sys})^2 + (W_* - W_{\rm sys})^2} \quad (1)$$

where U is the Galactic radial-velocity component positive towards the Galactic centre, V is the Galactic rotational velocity component positive towards $l = 90°$, and W is positive towards the Galactic north pole. For circular rotation around the Galactic centre, the W component of the velocity is expected to be zero. We adopted $\alpha_{GC} =$ 17:45:37.2, $\delta_{GC} = -28$:56:10.23 for the Galactic centre and $\alpha_{GNP} =$ 12:51:26.3, $\delta_{GNP} =$ 27:07:42.01 for the Galactic north pole (Reid & Brunthaler 2004). We used the solar peculiar motion relative to the LSR of ($U_\odot = 10.6$, $V_\odot = 10.7$, $W_\odot = 7.6$) km s^{-1}, the velocity of the LSR relative to the Galactic centre of 236 km s^{-1}, and a solar Galactocentric distance of 8.15 kpc based on the A5 fit provided by Reid et al. (2019). For the computation of the peculiar velocity, for

[2] http://stev.oapd.inaf.it/cgi-bin/cmd

each star the position, distance, proper motion and radial velocity (if available) were used. If the radial velocity was not available, we adopted zero for the peculiar radial-velocity component; this may lead to an underestimation of $V_{\rm pec}$.

We also calculated the motion of the young clusters with respect to the LSR; one would expect that they are at rest with respect to the Galactic rotation model, but e.g. Comeron et al. (1998) showed that the young stellar population in the solar environment can deviate from this model by up to 20 km s^{-1}. We applied the same approach to the young clusters as we did for the OB stars, calculating the mean relative velocity of their members. Since the radial velocities of the clusters are unavailable, we computed their mean tangential velocities relative to the LSR, along with 1σ uncertainties (see Column 8 of Table 1). The results indicate that the clusters' motion relative to the LSR is similar to that of Vel OB1 (~10 km s^{-1}, Section 2.2.1), which is another indication that the young clusters are part of Vel OB1.

Of the 77 objects listed in Table A.1 we determine a peculiar velocity $v_{\rm pec} \gtrsim 30$ km s^{-1} for 12 of them. The relatively flat distribution of tangential velocities among the runaway stars (Fig. 2 right panel) provides the basis for proposing a revised threshold for the peculiar velocity. Adopting $v_{\rm pec} \gtrsim 15$ km s^{-1}, the number of candidate runaways increases to 22. For some objects $v_{\rm pec}$ differs depending on whether this velocity is measured with respect to the LSR velocity or to Vel OB1. If the object is located relatively far away from Vel OB1, one should take the value of the peculiar velocity with respect to the LSR there. We confirm the runaway nature of the 7 objects in common with Carretero-Castrillo et al. (2023) (bold face in Table A.1; we note that HD 298429 has $v_{\rm pec} \simeq 20$ km s^{-1}).

3.2. Runaways associated with a wind bow shock

We have searched for arc-like features in the region of Vel OB1 that may be due to a wind bow shock produced by an OB runaway star. These bow shocks are relatively large features (arcminute size, parsec scale) and an indication for the (supersonic) motion of the OB star with respect to the ISM (van Buren & McCray 1988). Wind bow shocks associated with massive stars radiate primarily at mid-infrared wavelengths, where thermal emission from dust grains heated by the intense ultraviolet (UV) radiation of the OB star dominates (Comeron & Kaper 1998; Meyer et al. 2014; Henney & Arthur 2019). A well-studied illustration of this phenomenon is the bow shock surrounding the high-mass X-ray binary HD 77581 (Vela X-1), which has been detected and characterised across multiple wavelength regimes (Kaper et al. 1997; van den Eijnden et al. 2022). Fig. 3 presents a *Spitzer* colour-composite image of this runaway system (Iping et al. 2007). The wind bow shock around Vela X-1 is aligned with the direction of proper motion. Apart from *Spitzer* Space Telescope data using the *Spitzer* Infrared Array Camera (IRAC, Fazio et al. 2004) centred at 3.6, 4.5, 5.8, and 8.0 µm and the Multiband Infrared Photometer of *Spitzer* (MIPS) at 24 µm (Carey et al. 2009), we also used Wide-field Infrared Survey Explorer (WISE, Wright et al. 2010) data in the 3.4, 4.6, 12, and 22 µm band pass.

We explored the AllWISE survey in the field contained by Vel OB1 for the presence of arc-like structures that could be due to a wind bow shock. Fig. 4 presents the infrared colour-composite AllWISE images of 17 arc-like features (excluding Vela X-1) that often turn out to be associated with an OB star in Vel OB1 (though not all included in the compilation of Reed (2000), cf. Table A.1). Four of these arc-like features – HD 76031, GSC 08152-02059, DR3 N72, and DR3 N60 – are

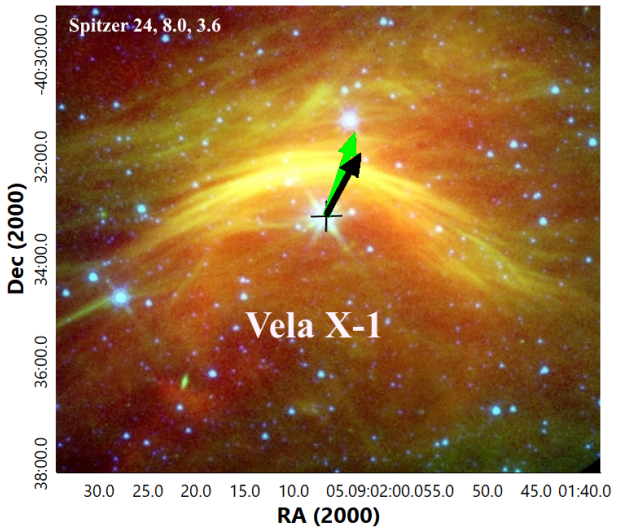

Fig. 3. *Spitzer* colour-composite image of the Vela X-1 system. The runaway star is marked with a cross. The black arrow indicates the direction of the current proper motion of the system. The green arrow exhibits the orientation of the wind bow shock, i.e. the direction from the star to the peak of the 22 μm emission.

reported here for the first time (see Appendix D for notes on individual objects. The white arrow indicates the direction of the observed proper motion of the stars. The green arrow highlights the orientation of the bow shock, i.e. the direction from the star to the peak of the 22 µm emission. Often these two arrows are not precisely aligned, i.e. the apparent motion of the star is not aligned with the opening angle of the arc-like structure. Obviously projection effects could play a role, as well as the bulk velocity of the ISM. Based on HIPPARCOS observations Kobulnicky et al. (2016) measured a relatively wide distribution of misalignment (up to 180 degrees) for a sample of 286 infrared bowshocks. Similarly Bodensteiner et al. (2018) found that 64% of 94 bow shocks are misaligned (>20 °). We will return to this point in Sect. 5.

For each bow shock we looked for a stellar counterpart (Table A.2); the large majority are early-type stars in the distance range occupied by the Vel OB1 association. Some objects may be too distant to be related to Vel OB1. The peculiar or transverse velocity of the stars associated with a bow shock (column 10 in Table A.2) indicates that some of them are "classical" OB runaway stars (e.g. Blaauw 1961; Boubert & Evans 2018) with a large, and very likely supersonic space velocity such that a wind bow shock is produced. Others may be termed walkaways (<30 km s^{-1}, Renzo et al. 2019); the inclusion of the radial velocity may change this result. Some of the OB runaway candidates associated with a bow shock have a modest space velocity ($\simeq$10 km s^{-1}), but that may still be supersonic (Sect. 5).

Based on the images in Figs. 3 and 4 and the information in Table A.2, we conclude that for 10 objects the arc-like feature most likely refers to the presence of a wind bow shock. Among the confirmed OB runaways in Vel OB1 (excluding candidate runaways in the projected field), the aligned cases are predominantly associated with higher peculiar velocities, while misaligned cases tend to have lower peculiar velocities (Fig. 9). This trend is a direct physical prediction of bow shock theory: at higher Mach numbers, the ram pressure of stellar motion dominates over ISM thermal and turbulent pressure, producing a well-defined shock tightly aligned with the space velocity. Conversely, at lower peculiar velocities – where the

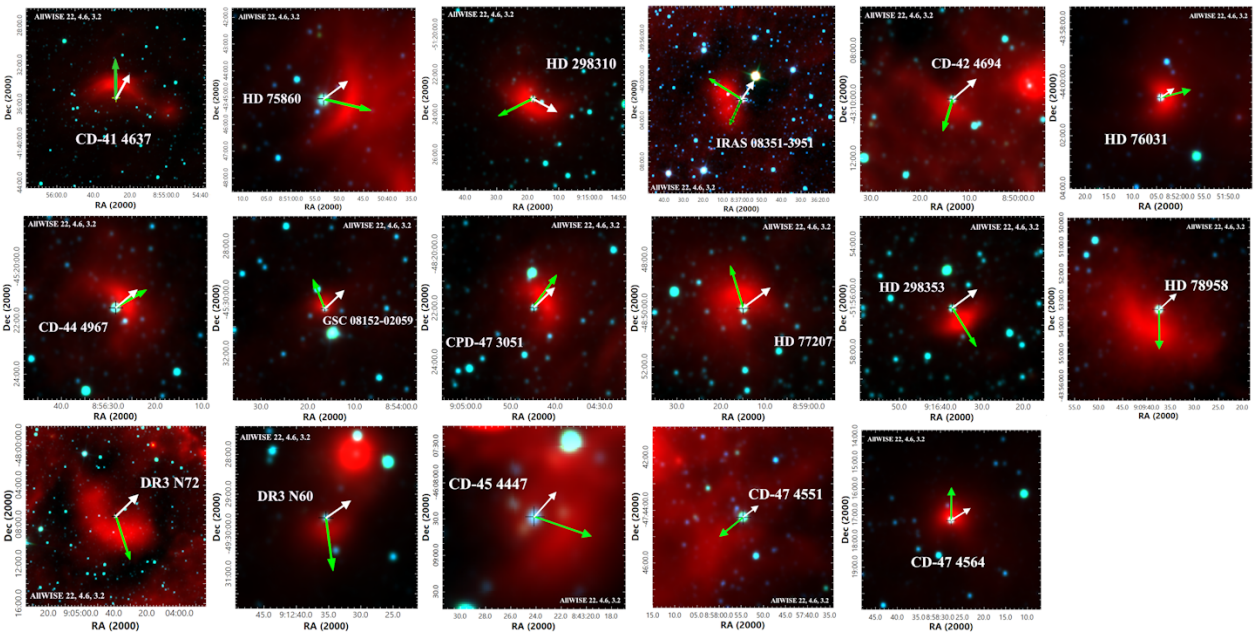

Fig. 4. AllWISE colour-composite images of arc-like structures associated with (OB-type) stars in the Vel OB1 region. The star is identified with the white label (and a cross), and the infrared flux is represented by the heat colour scale. The white arrow shows the direction of the current proper motion of each star. The green arrow indicates the orientation of the wind bow shock, i.e. the direction from the star to the peak of the 22 μm emission. In ten cases (including HD 77581 / Vela X-1, Table A.2), the arc-like structure is well aligned with the direction of the proper motion, demonstrating that these structures relate to a wind bow shock (and confirming the runaway nature of the star).

star is only marginally supersonic – ISM density gradients, bulk flows, and turbulence can distort the shock orientation, naturally producing a wide range of misalignment angles. Crucially, this V_{pec}–alignment correlation would not be expected if the arc-like features were randomly oriented ISM structures coincidentally aligned with stellar motion in the aligned cases. A Fisher's exact test comparing the fraction of aligned bow shocks among high-velocity ($V_{pec} \geq 15$ km s^{-1}) versus low-velocity systems gives $p \approx 0.17$, which does not reach formal significance given the small sample of 16 objects. Nevertheless, the direction of the trend – four out of five high-velocity systems aligned versus six out of 11 low-velocity systems – is consistent with the physical prediction of bow shock theory, and the limited statistical power reflects the sample size rather than the absence of a real physical effect.

Additional physical support for the bow shock interpretation comes from the consistency between the ISM number density derived independently (see Section 5) from the standoff distance (using the Baranov et al. (1971) pressure balance, Eq. (2)) and from the Strömgren sphere radius (Eq. (3)). For most sources in Table 2, these two independent estimates agree to within a factor of a few, indicating that the same star is responsible for both the ionisation of the surrounding medium and the wind-ISM interaction producing the arc-like feature. This consistency provides strong evidence that the observed structures are genuine wind bow shocks rather than unrelated ISM features. The remaining 8 arc-like features that are misaligned with the stellar proper motion (angle >70°) may be attributed to: (1) in situ bow shocks shaped by bulk ISM flows rather than stellar motion, as proposed by Povich et al. (2008); Bodensteiner et al. (2018) and observed in e.g. Guarcello et al. (2025); (2) wind-ISM interactions distorted by density gradients perpendicular to the stellar velocity, which cause the bow shock to become asymmetric (Wilkin 2000); or (3) unrelated ISM structures, as appears to be the case for CD-47 4551 and IRAS 08351-3951 (labelled ISM in Table A.2), which are included in the count of 18 arc-like features but excluded from the bow shock alignment statistics. Two additional objects – HD 71649 and HD 78927 – show arc-like emission in the AllWISE images but no reliable bow shock angle could be measured and they are not included in the bow shock sample. Excluding CD-47 4551 and IRAS 08351-3951 reduces the bow shock sample to 16, with ten aligned and six genuinely misaligned cases. We note that several confirmed runaways – including HD 76031, HD 77207, CPD-47 3051, and CD-47 4564 – have peculiar tangential velocities below the 15 km s^{-1} threshold and are identified as runaways primarily on the basis of their associated bow shock. Indeed, some of these stars have peculiar velocities below the local ISM sound speed (10–15 km s^{-1}), meaning that their stellar motion alone is insufficient to drive a supersonic bow shock. In these cases, large-scale flows in the ISM – potentially driven by cluster winds – must provide the additional relative velocity between the star and its environment (Povich et al. 2008; Bodensteiner et al. 2018), and the misalignment of the arc-like feature with the stellar motion is then a natural consequence. Nevertheless, for three of these stars, the consistency between the standoff distance and Strömgren sphere density estimates in Table 2 provides independent physical confirmation that these stars are indeed moving supersonically through the local ISM, likely due to such large-scale ISM flows contributing to the relative velocity. In the Appendix (Fig. C.1) we show AllWISE images centred on the OB runaways that we identified based on their peculiar velocity (and are not displayed in Fig. 4). Thus, a significant number of OB runaways apparently do not produce a wind bow shock; see also Huthoff & Kaper (2002); Carretero-Castrillo et al. (2025).

3.3. Properties of the OB runaways

Table A.2 lists the astrometric and kinematic properties of the OB runaway stars. Their peculiar velocity ranges between a few

Table 2. Adopted and estimated parameters of the observed bow shock around the runaway stars.

Runaway	l	b	V_w	$\dot{M}$	n_{ISM}^{BS}	n_{ISM}^{St}	R_{St}	R
–	(deg)	(deg)	($km\,s^{-1}$)	($M_\odot\,yr^{-1}$)	(cm^{-3})	(cm^{-3})	(°)	(arcsec)
(1)	(2)	(3)	(4)	(5)	(6)	(7)	(8)	(9)
CD-41 4637	263.02	2.30	$2250^{(e)}$	$6.9\times10^{-6(e)}$	30	28	0.26	90
HD 77581/Vela X-1	263.06	3.93	$700^{(a)}$	$6.3\times10^{-7(a)}$	1.0	3.7	0.27	53
HD 75860	264.14	0.27	$(700-800)^{(d)}$	$(1.6\times10^{-7}-7.6\times10^{-6})^{(d)}$	(0.6–34)	4.3	*0.08*	59
HD 76031	264.50	0.30	$(300-1200)^{(f)}$	$(10^{-9}-10^{-8})^{(f)}$	(0.7–26)	17	*0.05*	11
CD-44 4967	266.01	0.00	–	–	–	–	0.18	29
CD-47 4564	268.46	−1.65	$(900-1100)^{(d)}$	$6.4\times10^{-8(d)}$	(31–38)	13	0.07	8**
HD 77207	268.96	−1.90	$500^{(b)}$	$1.5\times10^{-7(b)}$	35	–	0.10	32
CPD-47 3051	269.21	−0.91	$1200^{(b)}$	$7.7\times10^{-9(b)}$	13.5	14	0.10	28
HD 298310	272.58	−1.72	$1200^{(b)}$	$3.4\times10^{-7(b)}$	4.0	8.2	0.16	21
CD-42 4694	263.61	0.55	$(1140-1300)^{(e)}$	$(10^{-7}-10^{-9})^{(e)}$	(0.3–25)	*70*	*0.05*	18
CD-45 4447	265.18	−2.26	$(1745-2390)^{(c)}$	$(3.6\times10^{-8}-1.1\times10^{-7})^{(d)}$	(130–560)	*91*	*0.02*	22**
GSC 08152-02059	265.88	−0.39	–	–	–	–	*0.06*	15**
HD 78958	266.47	2.73	$(500-2000)^{(c)}$	$3.0\times10^{-6(e)}$	(809–3236)?	14	0.10	40**
DR3 N72	269.01	−0.76	–	–	–	–	0.13	34**
DR3 N60	270.91	−0.73	–	–	–	–	*0.10*	19**
HD 298353	273.12	−1.96	$2500^{(b)}$	$6.0\times10^{-8(b)}$	25	41	0.10	32

Notes. (1) name of star, (2), (3) Galactic coordinates of star, (4) adopted terminal wind velocity, (5) adopted mass-loss rate, (6) ambient interstellar number density determined by the balance between the ram pressures of the wind and the ambient medium (Baranov et al. 1971) computed in this work, (7) ambient interstellar number density determined by the relationship of Lequeux (2005) computed in this work, (8) the putative Strömgren radius obtained from *WISE* 22 μm image of the region, (9) standoff distance from Kobulnicky et al. (2016). The parameters are taken from Giménez-García et al. (2016) (a); Kobulnicky et al. (2019) (b); Prinja et al. (1990) (c); the parameters are based on the spectral type Kobulnicky et al. (2019) (d); Mokiem et al. (2007) (e); typical value for early-B subgiants Krtička (2014) (f); (**) we measured the standoff distance in the WISE 22 μm images. Two objects are indicated as DR3 N72 and N60 based on their last numbers of `source_id` from *Gaia* DR3. Suspicious results are in *italic*. Candidate runaway systems are listed in the bottom part of the table.

to over a hundred km s^{-1} (Column 10 in Table A.2). The tangential velocity distribution of the OB runaways is relatively flat (Fig. 2) and similar to that of the runaways presented in Carretero-Castrillo et al. (2023) and Stoop et al. (in prep.). We conclude that 8 out of 77 OB stars in Vel OB1 are runaways with a peculiar tangential velocity exceeding 30 $km\,s^{-1}$; 15 runaways move faster than 15 $km\,s^{-1}$, i.e. with respect to the LSR (and thus also relative to the young clusters in Vel OB1). If we also take into account the radial velocity (if available) we find that 14 or 21 (+1 F-type) OB runaways have a peculiar velocity greater than 30 or 15 km s^{-1}, respectively, yielding a runaway fraction of 18 or 29%, respectively. Seven of the 26 identified OB runaways (including HD 77581, the companion to the X-ray pulsar Vela X-1) are in common with the list of Galactic OB runaways in Carretero-Castrillo et al. (2023), i.e. all seven OB runaways that they report in the field of Vel OB1 that we studied.

Most OB runaways identified in the Vel OB1 region are of spectral type O (8/26) or B (17/26); only HD 74920 is a luminous F2 supergiant located more than 100 pc below the Galactic plane. The runaway fraction as a function of spectral type then becomes 38% for the O stars (8/21) and 32% (17/52) for the B stars. If we count the B supergiants only, we arrive at a runaway fraction of 24% (6/25). Four out of eleven OB supergiants are associated with a wind bow shock.

Two OB runaways are member of a HMXB: HD 77581 (BP Cru) with its X-ray pulsar companion Vela X-1 (Kaper et al. 1997) and HD 74194 (LM Vel) that is associated with the supergiant fast X-ray transient IGR J08408-4503 (Gamen et al. 2015). HMXBs are expected to be runaway systems produced by the binary supernova scenario (van den Heuvel et al. 2000); both systems are included in the studies of Carretero-Castrillo et al. (2023) and Fortin et al. (2022) and are confirmed as runaways.

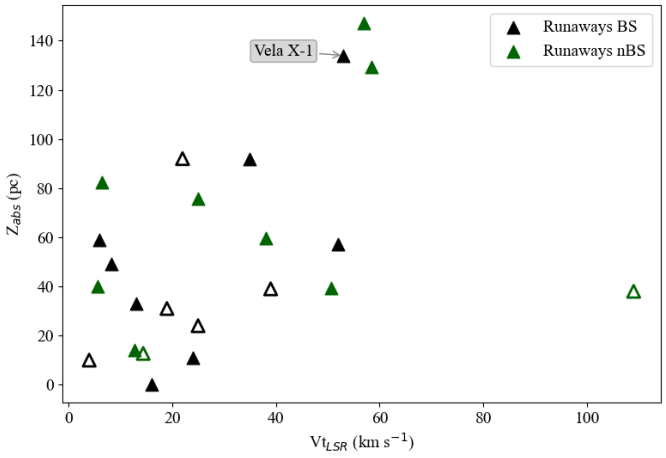

Fig. 5. Galactic height Z_{abs} versus the peculiar transverse velocity of the OB runaways in Vel OB1. Open triangles refer to candidate runaways (see Table A.2). It shows the expected trend that the fastest runaways reach the largest distance from the Galactic plane. Ten of the OB runaways with an observed bow shock are within 60 pc from the Galactic plane where most of the gas and dust is present. Vela X-1 is at a height of 134 pc and still produces a prominent wind bow shock.

The Galactic height Z of the OB runaways ranges from 0 to almost 150 pc above the plane. The OB runaways at a larger distance from the plane typically have a larger space velocity (Fig. 5). Also, most (10) OB runaways with an associated bow

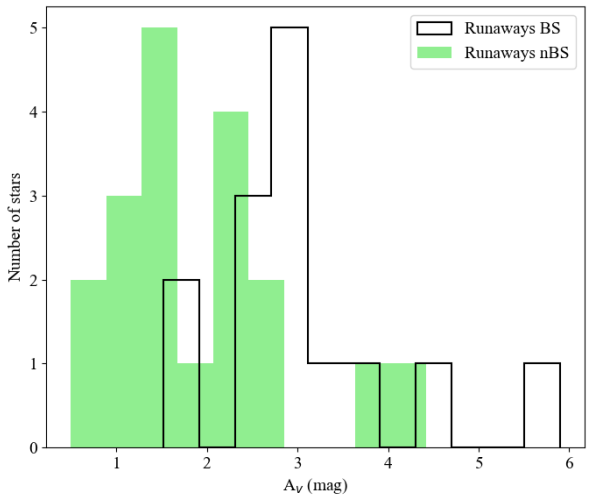

Fig. 6. Extinction, A_V, measured in the sight lines towards the OB runaways with (black histogram) and without an associated wind bow shock (green histogram). The OB runaways with a bow shock experience a higher extinction than those without a bow shock.

shock are found within 60 pc from the Galactic plane where the interstellar gas and dust are predominantly concentrated. An exception is Vela X-1 which is located at 134 pc above the plane and still manages to produce a prominent wind bow shock. It should be noted, however, that large-scale infrared and radio images suggest that Vela X-1 passed through an over-dense ridge in the ISM $\sim 10^5$ years ago, where it may have swept up a significant amount of gas (Gvaramadze et al. 2018; van den Eijnden et al. 2022).

Despite their high space velocity, we did not observe a bow shock for the majority of the OB runaway stars identified by their high peculiar velocity (Table A.2 and Fig. C.1). This could be related to the conditions of the ambient medium through which they travel (cf. Sect. 5).

For the runaways with an accurate spectral type we derive the intrinsic colour $(B-V)_0$ and, with this information, estimate the interstellar extinction. Fig. 6 presents a histogram of the visual extinction A_V (adopting $R_V = 3.1$) demonstrating that A_V in the line of sight of these runaways is in the range between 0.5 to 6 mag. The OB runaways for which a wind bow shock has been detected have an on average higher extinction than those without a bow shock. This may indicate that a wind bow shock is formed if the OB runaway moves through denser regions of the ISM, and is also consistent with the observation that OB runaways with a bow shock are more confined towards the Galactic plane (Sect. 5).

Fig. 7 displays the location of the OB runaways (triangles) in the colour-magnitude diagram with respect to the young cluster RCW 38 (blue) as a reference. Clearly, the OB runaways are more luminous than most of the cluster members; correction for the interstellar extinction would move them to the top-left side of the diagram. The right panel in Fig. 7 shows the position of the OB runaways in the Hertzsprung-Russell diagram (HRD). The effective temperature is derived from the spectral type, and the luminosity has been determined using the distance (*Gaia* parallax), the bolometric correction and the extinction. Most OB runaways are likely still in the hydrogen-burning phase; some others may already be on their way to become a red supergiant.

As soon as a parent cluster has been identified, one would know the age of the runaway (assuming that it was born in the cluster) if the runaway is the result of dynamical ejection. If the binary supernova scenario produced the runaway, the evolutionary state of the OB runaway depends on whether mass transfer occurred prior to the supernova explosion. In cases where the primary transferred a significant amount of mass to the secondary before undergoing core collapse, the secondary gains mass and luminosity, making it appear younger than the cluster population – a so-called blue straggler (rejuvenation; e.g. van den Heuvel et al. 2000; van der Meij et al. 2021). In systems where no mass transfer took place, the companion is simply accelerated by the supernova kick and remains a normal star consistent with the cluster age. For Vela X-1, van Rensbergen et al. (1996) proposed a phase of mass transfer prior to the supernova, so one would expect that its B-supergiant companion HD 77581 is located at a more luminous and bluer location than the isochrone corresponding to the age of the parent cluster.

4. Identifying the parent cluster of the OB runaway stars

In order to identify the potential parent cluster of an OB runaway we use its current motion to find out whether its path originates in one of the (young) clusters embedded in Vel OB1. One also needs to take into account the motion of the cluster. For each OB runaway Fig. 8 shows the path that was followed during the past Myr; here we assume that the Galactic potential has not changed the direction of motion significantly. The path of RCW 38 is indicated by the dashed red line. The direction and pace along this path is representative for all young clusters listed in Table 1.

The general conclusion based on Fig. 8 would be that the large majority of the OB runaways originate in the Galactic plane. In a few cases, we think that we can identify the parent cluster of the OB runaway (Table A.3). Recent observational studies suggest that a large fraction of OB runaways originate in young stellar clusters located in the Galactic plane and are ejected during, or shortly after, the cluster formation phase (e.g. Gvaramadze et al. 2011; Drew et al. 2021; Maíz Apellániz et al. 2022; Stoop et al. 2023, 2024b). For these objects, the time elapsed since ejection – referred to as the kinematical age – is therefore expected to be comparable to the age of the parent cluster. In contrast, if a runaway star is produced through the binary supernova channel, the kinematical age is typically much shorter than the cluster age, since the system must first evolve until the supernova occurs; an illustrative example is discussed by van der Meij et al. (2021).

For five OB runaways, we identified the potential parent cluster (top five systems in Table A.3): HD 75222 (Bochum 7), CD-41 4637 (RCW34), GCS 08152-02059 (RCW38), HD 76968 (Bochum 7), and HD 298310 (RCW38). For more information on these systems, see Appendix D.

Fortin et al. (2022) searched for the birth place of a sample of HMXBs, including HD 74194 / IGR J08408-4503 and HD 77581 / Vela X-1. For both systems they cannot identify a parent cluster. Tracing back the path of these systems shows that they would have intersected with the Local arm several tens of Myr ago, too long ago compared to the expected age of these systems. Fortin et al. (2022) conclude that these systems may have formed in isolation. Alternatively, the path of HD 74194 (LM Vel) may originate in the open cluster [FSR2007] 1452, which would result in a kinematical age of about 4 Myr; however, Tarricq et al. (2021) report a cluster age of ~260 Myr which would be too old to be the parent cluster of this HMXB. We return to the case of Vela X-1 in Sect. 6.3.

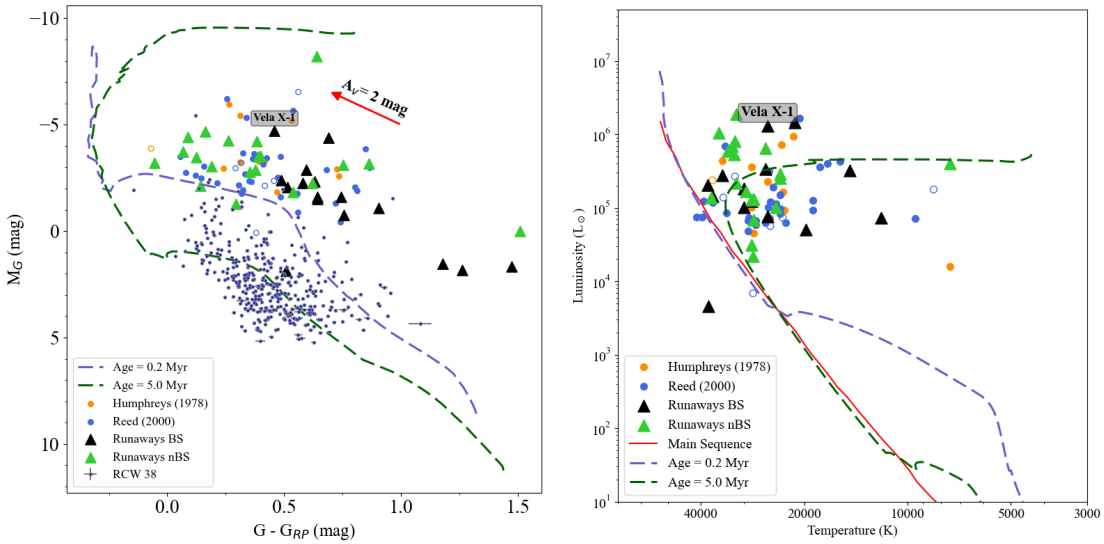

Fig. 7. *Left panel*: OB runaways originating in Vel OB1 and the candidate members of Vel OB1 (neither has been corrected for interstellar extinction) plotted in the colour-absolute magnitude diagram of RCW 38. The OB runaways associated with a wind bow shock (black triangles) are more reddened than those without a bow shock (green triangles). The red arrow represents the dereddening vector. The PARSEC isochrones (dashed lines) are shown for an adopted reddening of A_V = 3 mag. *Right panel*: OB runaways and the candidate members in the HRD (with the effective temperature based on spectral type, luminosity based on distance, bolometric correction included, and corrected for extinction). The red line represents the zero-age main sequence from the solar metallicity grid in Maíz Apellániz (2013); the dashed lines are PARSEC isochrones corresponding to the age indicated in the legend. The location of the OB runaways suggests that most of them are still in the hydrogen-burning phase; some others are on their way to become a red supergiant.

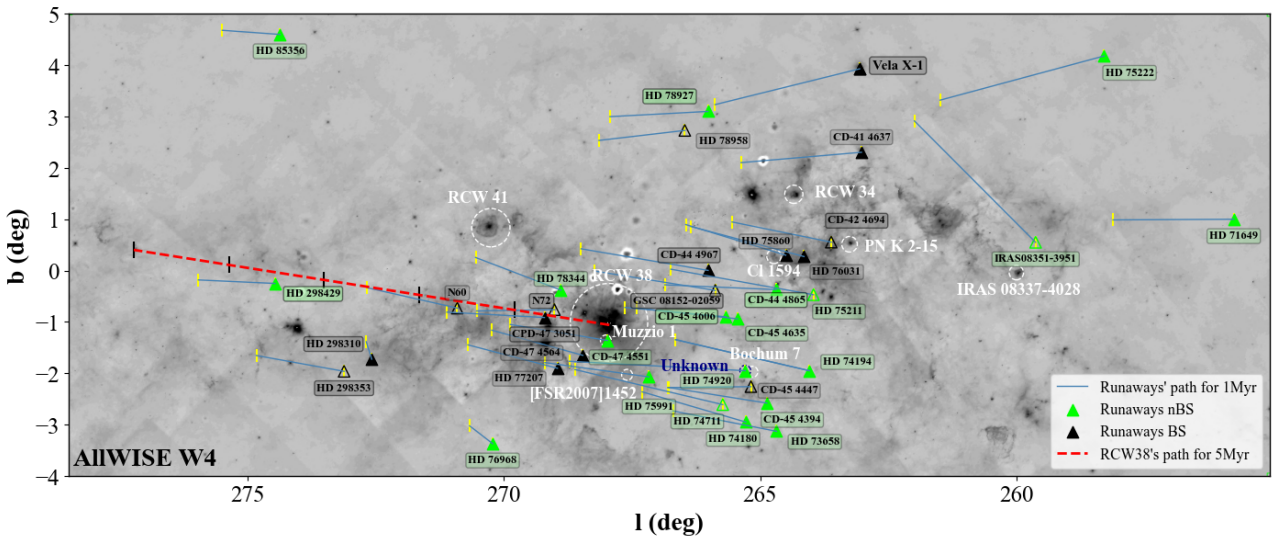

Fig. 8. AllWISE W4 image of the Vel OB1 association showing the positions of the OB runaways with (black triangles) and without an associated bow shock (green triangles). The OB runaways and the potential parent clusters are labelled (white). The dashed red line shows the path of RCW 38 traced back over 5 Myr. This motion can assumed to be representative for the motion of the other young clusters in this association. The blue lines display the path of each OB runaway up to 1 Myr ago. The [KPS2012] MWSC 1594 open cluster is refered to as Cl 1594. For a handful of OB runaways an origin in one the young clusters is likely; most OB runaways seem to originate from the Galactic plane.

Possibly the pulsar PSR J0858-4419 has been the companion to one of the identifed OB runaways in Vel OB1 before the supernova explosion. The galactic coordinates of PSR J0858-4419 are 265.45724;+00.82166; the proper motion of the pulsar has not been measured, but the distance estimate of 1.9 kpc (Romani et al. 2011; Krishnakumar et al. 2015) is in accordance with Vel OB1 (though the alternative distance of 6.5 kpc reported by D'Amico et al. (1998) would not fit to this scenario).

As already mentioned, most OB runaways in Vel OB1 move away from the Galactic plane. In Table A.3 we list the time it took to cross Galactic latitude b = 0, 1, and 2 degrees: the conclusion is that these OB runaways, if born in the Galactic plane, escaped typically a few Myr ago to reach their current position.

5. Wind bow shocks and ISM conditions

For eight out of the 25 OB runaways (32%) in Vel OB1 an arc-like feature has been detected most likely due to the presence of a wind bow shock. This percentage is in line with the findings of Carretero-Castrillo et al. (2025) that ~24% of their O-type

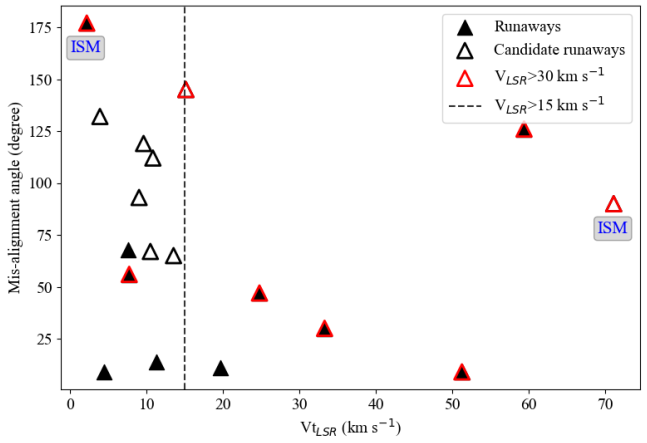

Fig. 9. Alignment (or misalignment) angle between the proper motion vector of the system and the symmetry axis of the bow shock as a function of the peculiar tangential motion. We have classified the bow shock as 'aligned', 'aligned?', and 'misaligned' following the criteria listed in Kobulnicky et al. (2016) (see text); CD-47 4551 and IRAS 08351-3951 are identified as unrelated ISM structures and excluded from the bow shock sample (see text). The misalignment angle shows a wide range for those systems with a low peculiar velocity.

runaways produce a bow shock. Another observation is that the OB runaways producing a bow shock experience a higher visual extinction (Fig. 6) indicating that their ambient medium has a higher density (of dust). This is not unexpected as, besides the higher than average dust density near the Galactic plane, the formation of a wind bow shock depends on the ISM density.

We also measured the (mis)alignment angle between the (proper) motion of the system and the symmetry axis of the bow shock (Fig. 9). The uncertainty of the misalignment angle is difficult to judge: it largely depends on the observed symmetry of the arc-like feature and the assumption that the maximum 22 μm emission refers to the top of the bow shock. Assuming a 5° uncertainty for the bow-shock position angles from Kobulnicky et al. (2016) and propagating Gaia proper-motion uncertainties including covariance terms, we obtain a typical misalignment-angle uncertainty of ∼5°. In contrast, Kobulnicky et al. (2016) applied a conservative cut on the uncertainty of the proper-motion position angle (<45°) rather than estimating the uncertainty in the misalignment angle itself. It turns out that OB runaways with a relatively low peculiar velocity show a wide range in alignment (up to total misalignment), while the bow shocks associated with systems with a high peculiar velocity show better alignment with the proper motion vector. We divided the observed bow shocks in two morphology groups: aligned and misaligned, based on the measured misalignment angle. If the misalignment angle is <45°, the bow shock is considered aligned (e.g. Kobulnicky et al. 2016; Bodensteiner et al. 2018); if the misalignment angle is >45° and <70°, the bow shock is considered aligned with a question mark (considering the contribution of the proper motion errors). In other cases (>70°), it is mis-aligned. This means that the apparent motion of the star is not aligned with the opening angle of the nebula. Of the 18 arc-like features, two objects – CD-47 4551 (misalignment angle 177°) and IRAS 08351-3951 (90°) – are identified as unrelated ISM structures (labelled ISM in Table A.2) and are excluded from the bow shock alignment statistics. Thus, among the remaining 16 bow shock candidates, we have ten aligned (including those with a question mark) and six misaligned bow shocks, respectively.

The observed stand-off distance of a wind bow shock is determined by the equilibrium between the momentum flux of the stellar wind and the ram pressure of the surrounding ISM (Baranov et al. 1971). We can confirm whether the observed arc-like feature is due to a wind bow shock based on the stellar parameters and the local ISM conditions. This is relevant, as several of our OB runaways are identified on the basis of the association with a bow shock, while their peculiar velocity is lower than our tangential velocity threshold of 15 km s^{-1}. In these cases, large-scale flows in the ISM – potentially driven by cluster winds – may produce a substantial relative velocity between the star and its environment (Povich et al. 2008; Bodensteiner et al. 2018).

Using the spectral type of the OB star, we estimate the wind mass-loss rate and terminal velocity from empirical prescriptions (Howarth & Prinja 1989; Kudritzki & Puls 2000). Given the stellar wind properties, the measured stand-off distance, and the peculiar velocity, the ambient ISM density remains the only unconstrained parameter (Baranov et al. 1971):

$$\rho_{\rm ISM} = \frac{\dot{M} V_{\rm w}}{4\pi V_{\rm pec}^2 R^2}, \tag{2}$$

where $\rho_{\rm ISM}$ is the density of the ISM, equal to 1.4 $m_{\rm H} n_{\rm ISM}$, $m_{\rm H}$ is the mass of the hydrogen atom, $\dot{M}$ is the stellar wind mass-loss rate, $V_{\rm w}$ is the terminal wind velocity, $V_{\rm pec}$ is the (peculiar) velocity of the star with respect to ISM and R is the stand-off distance, i.e. the projected closest distance between the star and the bow shock. For five runaway stars $V_{\rm w}$ and $\dot{M}$ have been reported in literature (see Table 2). For the remaining stars $V_{\rm w}$ and $\dot{M}$ are estimated by taking the average value for stars of the same spectral type (Kobulnicky et al. 2019; Mokiem et al. 2007). As a result, we obtain a value of $n_{\rm ISM}$ (Table 2).

Another way to estimate $n_{\rm ISM}$ is through the size of the extended H II region powered by the UV emission of the star; this provides a consistency check on the derived value of $n_{\rm ISM}$ based on the stand-off distance of the bow shock. The number density of the ambient medium can be obtained using the relationship (Lequeux 2005)

$$R_{\rm Str} = \left[\frac{3S(0)}{4\pi n_{\rm ISM}^2 a}\right]^{1/3}, \tag{3}$$

where $R_{\rm Str}$ is the radius of Strömgren sphere (Strömgren 1939), $S(0)$ the ionising flux emitted by the star (Panagia 1973) and a the recombination coefficient ($a = 3.4 \times 10^{-13}$ cm^3 s^{-1} for T$_e$ = 7000 K typical for H II regions, see Lequeux 2005).

As an example we take the case of HD 77581 / Vela X-1: Figure 10 shows the *WISE* 22 μm image of the region including the B supergiant HD 77581 with the position of the putative Strömgren sphere indicated by a dashed white circle (see also Gvaramadze et al. 2018). It corresponds to the angular radius of the green contour where the 22 μm flux exceeds the background surface brightness by 3σ (a bit larger area than noted by Kaper et al. 1997). The position of the bow shock generated by HD 77581 is indicated by a black contour. If this extended infrared source is indeed an ionisation-bounded H II region created by the UV emission of the OB runaway star, we obtain $R_{\rm Str} = 0.27°$ and $n_{\rm ISM} = 3.7$ cm^{-3} (Eq. (3)). When we adopt the values for $\dot{M}$ and V$_w$ reported for HD 77581 (Giménez-García et al. 2016) and the observed stand-off distance of the wind bow shock, we arrive at $n_{\rm ISM} = 1.0$ cm^{-3}, in reasonable agreement with the value based on the estimate of $R_{\rm Str}$ (Table A.2) and

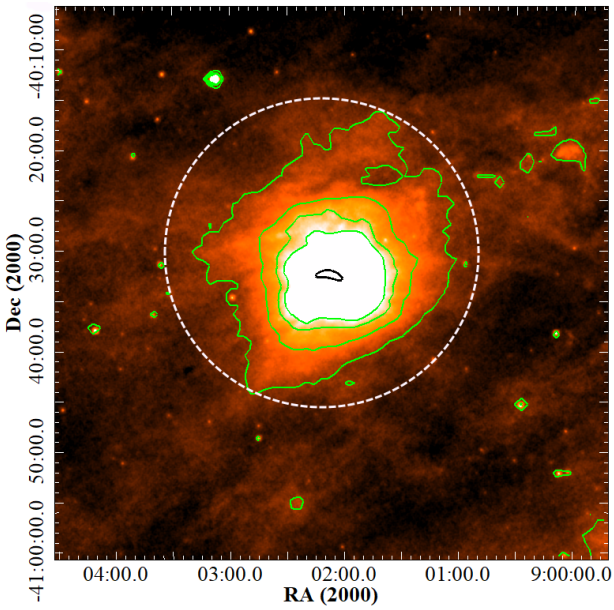

Fig. 10. *WISE* 22 μm image of the field containing Vela X-1. The position of the bow shock generated by Vela X-1 is indicated by a black contour. The area surrounded by a dashed white circle of radius of 0.27° corresponds to the putative Strömgren zone produced by Vela X-1. The external green contour corresponds to 3σ of background surface brightness.

the ambient interstellar number density adopted by Kaper et al. (1997).

We used *WISE* 22 μm images for the identification of the putative Strömgren sphere for the other stars. In some cases, the identification of the putative Strömgren sphere is not clear because the object is embedded in a complex region. Table 2 lists the results; for some runaways, we lack information. In most cases we find reasonable agreement between the two estimates of the ISM number density, suggesting that the Strömgren sphere and the bow shock are produced by the same star. In other cases the discrepancy could be due to the underestimated relative velocity as we assumed that the ISM is at rest with respect to the Galactic rotation. The derived values of the ambient-medium density around HD 77581, CD-41 4637, HD 77207, and HD 298353 stars are fairly high for what one would expect at these Galactic heights (see Columns 8–9 in Table 2). The observations at longer wavelengths (>22 μm), however, indicate the presence of a relatively dense medium surrounding these stars. In general we find good agreement between the two determinations of the ISM number density and the measurements of Kobulnicky et al. (2019) for individual stars. We conclude that the measured ISM number density is in the range of 0.1–40 cm^{-3}. We derived the mass-loss rate of the OB runaways using n^{St}_{ISM} in Eq. (2) (see Column 7 in Table 2). The derived mass-loss rate is compatible with the adopted mass-loss rate. This is in accordance with the findings of Patten et al. (2025) regarding the parameters of the central stars of 103 infrared bow shock nebulae, but see Sect. 3.2.

The agreement between n^{BS}_{ISM} and n^{St}_{ISM} for most sources (Table 2) provides an independent consistency check on the bow shock interpretation. If the arc-like feature were an unrelated ISM structure, there would be no reason to expect its stand-off distance to be consistent with the pressure balance between the known stellar wind parameters and the local ISM density inferred from the Strömgren sphere. Eight of the 11 sources with both estimates available agree within a factor of three, strongly supporting the identification of these features as genuine stellar wind bow shocks.

6. Discussion

We have searched for OB runaways in the region contained by the Vel OB1 association, host of close to a hundred OB-type stars, at a distance of about 1.8 kpc. We characterised Vel OB1 by performing a membership analysis of a few young clusters included in the association. We identified OB runaways based on their peculiar motion (with respect to the LSR and to the mean motion of the young clusters, in some cases including the radial-velocity component) and/or the association with a wind bow shock. The definition of an OB runaway depends on the value of the peculiar-velocity threshold. We argue that a threshold of 15 km s^{-1}, which is still higher than the escape velocity of a stellar cluster, is sufficient to identify an OB runaway in this region.

6.1. Comparison to earlier work

6.1.1. Kinematical properties of the OB runaway stars

The OB stars in the sample studied by Carretero-Castrillo et al. (2023) (Galactic O-Star Catalogue and the Be Star Spectra Database) show a Gaussian peculiar tangential velocity distribution with a dispersion of 5–10 km s^{-1}. Their OB runaways have a (tangential) peculiar velocity in the range from 5 to about 150 km s^{-1}. Stoop (2024) demonstrate that their sample of over 400 OB runaways show a transverse velocity distribution (with tangential velocities in the range from 5 to 300 km s^{-1} with respect to their parent cluster) that can be modelled with a power law. The majority of the OB runaways has a tangential peculiar velocity in the range 5–20 km s^{-1}; note that these OB runaways are most likely produced by dynamical ejection.

Our Vel OB1 runaway sample shows a similar peculiar velocity distribution, rather flat (Fig. 5) and in the range between 5 and 70 km s^{-1}. The OB runaways identified by the association with a bow shock do not need to meet the tangential peculiar velocity threshold of 15 km s^{-1}, as long as they move at supersonic velocity. As argued in Sect. 5, these arc-like features are often misaligned with the direction of motion and may be the result of the interaction between a bulk flow of the ISM with the OB-star wind.

The distinction between runaway and walkaway stars (Renzo et al. 2019) is not sharply defined. While escape from the natal environment is ultimately governed by the cluster escape velocity, the traditionally adopted velocity threshold of 30 km s^{-1} does not have a strong physical basis. Binary evolution models show that the supernova ejection mechanism can produce a substantial number of systems with velocities well below this classical limit (Renzo et al. 2019), blurring the boundary between the two populations. Thus, all OB runaways observed in Vel OB1 can be produced by both mechanisms.

6.1.2. The OB runaway fraction

In Sect. 3.3 we report on 21 OB runaways on a total of 70 OB stars in Vel OB1 resulting in a runaway fraction of 29% (and 18% if we take 30 km s^{-1} as the threshold). The OB runaway fraction is higher for the O-type stars (38%) than for the B-type stars (32%). Carretero-Castrillo et al. (2023) report a percentage of 25% for O-type stars and 5.2% for Be stars. For about 24% of

the O runaways they detect a wind bow shock and for just about 3% of the Be runaways.

In a recent study of 15 young massive clusters Stoop (2024) find an OB-runaway fraction of 19% for the combined population of WN(h) and O-type stars, but this could be as high as ∼33% as a significant fraction of the OB runaways is lacking a spectral classification. As these OB runaways have a kinematical age less than 3 Myr and have an identified parent cluster, they are produced by dynamical ejection.

Pantaleoni González et al. (2025) present the third release of the Alma catalogue of OB stars (Reed 2003), cross-matched with *Gaia* DR3 and an extension based on new spectral classifications. Their list contains 583 stars in the direction of the Vel OB1 region; of them, 314 stars are at the same distance as Vel OB1. We compared Table A.1 with their list and all our 77 stars are in common. We also compared the OB runaway stars in Table A.2 (not included in Table A.1) with the list of Pantaleoni González et al. (2025) and 5 out of 8 stars are in common. Three stars, namely IRAS 08351-3951, DR3 N72, and DR3 N60 are not included in their list. It should be noted that IRAS 08351-3951 has spectral type M8 and that the spectral type of DR3 N72 and DR3 N60 are not known. Excluding the stars in common with the Alma catalogue, we searched for runaways with category "M" (likely massive stars) by measuring their tangential peculiar velocity. It turns out that 30 stars out of 211 have a tangential peculiar velocity higher than 15 km s^{-1}; these runaways are of spectral type O (2), B (13), A (2), G (1) and unknown (12). Adding them to our list of OB runaways (also from Table A.2), the runaway fraction as a function of spectral type then becomes 29% for the O stars (12/(21+20)) and 21% for the B stars (27/50+80).

We inspected the regions surrounding the new OB runaways based on the Alma catalogue and only ALS 1327 has a small arc-like feature associated with it. This star has a tangential peculiar velocity 63 km s^{-1}.

6.2. Dynamical ejection or binary supernova scenario

Two of the OB runaways are the optical counterpart of a HMXB: HD 77581 (Vela X-1) and HD 74194 (IGR J08408-4503). In some HMXBs, the system remains gravitationally bound following the supernova event that produces the compact object, while acquiring a systemic recoil velocity as a consequence of the mass lost during the explosion (van den Heuvel et al. 2000). For both systems no convincing parent cluster has been identified prohibiting a reconstruction of the evolutionary history of the system such as for HD 153919 (4U1700-37) (van der Meij et al. 2021). In exceptional cases an OB runaway can be traced back to a radio pulsar, indicating that the OB runaway was produced by the binary supernova scenario leading to the disruption of the binary progenitor system. Notable examples include the association of the OB runaway ζ Oph with PSR B1706-16 (e.g. Hoogerwerf et al. 2000; Neuhäuser et al. 2020), as well as the massive runaway star HD 254577 with the neutron star CXOU J61705.3+222127 (Dinçel et al. 2026).

For the OB runaways in Vel OB1 that could be linked to a parent cluster, the kinematical age is consistent with the estimated age of the parent cluster. For these runaways the dynamical ejection scenario is the most likely production mechanism. Thus, for the majority of the OB runaways in Vel OB1 the production mechanism cannot be determined. Both the dynamical ejection and the binary supernova scenario are at work, but in some cases also a hybrid scenario (a massive binary, dynamically ejected from a cluster, undergoes a supernova explosion at a later stage) could provide the explanation for the observed motion of the runaway.

6.3. A hybrid scenario for Vela X-1?

The formation history of the HMXB Vela X-1 remains uncertain. van Rensbergen et al. (1996) proposed that the initially more massive component, with an estimated mass of 25 $M_\odot$, underwent a supernova after at least 9 Myr, leaving behind a neutron star and the present-day 24 $M_\odot$ B-type supergiant companion. In this scenario, the system was ejected from the Vel OB1 association less than 3 Myr ago, implying a total system age of approximately 12 Myr. Using HIPPARCOS astrometry, Kaper et al. (1997) reached a similar conclusion regarding an origin in Vel OB1. Alternatively, Gvaramadze et al. (2018) suggested a two-step ejection process, in which the binary was first dynamically removed from its natal cluster through few-body interactions and later received an additional velocity kick from the supernova explosion after it had already travelled far from its birthplace.

Based on the Galactic latitude of Vela X-1 (b=+3.9°) and distance, its current location is 134 pc above the Galactic plane. We traced back the path of Vela X-1 HMXB and considered various scenarios to explain its current position and velocity. One of reconstructed paths of Vela X-1 reveals that its position on the sky was close the Vela R2 association about 2 Myr ago. However, the distance to Vela R2 is 850 pc (Eggen 1982), inconsistent with the current distance of Vela X-1 (∼1.9 kpc). Another option is that Vela X-1 left the RCW 38 region about 4.5 Myr ago; but then the total age of the system would be about 13 Myr (van Rensbergen et al. 1996). This is inconsistent with the age range of RCW 38 (3.2–7.1 Myr), unless this young cluster also hosts an older population (like M16, Stoop et al. 2023). Therefore, we consider a hybrid scenario as proposed by Gvaramadze et al. (2018) as the most likely scenario for Vela X-1. This is also concluded in the recent paper by Patten et al. (2025) where they looked at the fundamental parameters of the central (OB) stars of 103 infrared bow shock nebulae (Vela X-1 corresponds to BS386).

6.4. Impact on the surrounding medium

Massive OB stars strongly influence their surroundings through intense ultraviolet radiation, powerful stellar winds, and eventual supernova explosions, regardless of whether they remain in their natal clusters or migrate into the field. It is important to quantify the number and production rate of OB runaways. In this paper we attempt to obtain a census of the OB runaways in the massive star-forming region Vel OB1 using *Gaia* astrometric data and the association with a (wind) bow shock. While we identify approximately a dozen arc-like infrared features, not all of these structures necessarily arise from the supersonic motion of a runaway star. In some cases, the interaction between a fast bulk flow in the ISM and the wind of a relatively stationary OB star can produce similar morphologies (Bodensteiner et al. 2018; Kobulnicky et al. 2016). A comparable situation was reported by Guarcello et al. (2025), who identified a red supergiant in Westerlund 1 with a bow shock oriented away from the cluster centre, most likely shaped by large-scale ISM dynamics. Indeed we find indications that several arc-like features do not align with the measured space motion of a potential OB runaway, especially in case of runaways with a low peculiar velocity. Therefore, we need to be careful in identifying OB runaways based on their association with an arc-like ISM feature.

As runaway OB stars can traverse distances of hundreds of parsecs before exploding as supernovae, their feedback may be deposited far from their birth sites. In such low-density environments, supernova remnants can expand more freely, potentially allowing nucleosynthetically enriched material to escape the Galactic disc. The contribution of runaway stars to the heating, structuring, and chemical enrichment of the ISM – and possibly to Galactic outflows – may therefore be more significant than previously assumed (Andersson et al. 2020).

7. Summary and conclusions

The aim of this work was to search for OB runaway stars (and their associated wind bow shocks) in the Vel OB1 association, one of the largest OB associations known. We analysed six young stellar clusters contained in the Vel OB1 region, which make the majority of the massive-star population in this part of the Galaxy. We were able to identify 26 runaways by measuring their peculiar velocity with respect to the association. Moreover, we detected 16 arc-like features (bow shocks) in this region, four of them for the first time. We traced back the path of these objects to understand both the most likely cause for their acceleration (supernova of the companion star or the dynamical ejection from the parent cluster) and from which part of the Vel OB1 association the stars were kicked out. We identified the parent cluster for three runaways with observed bow shocks and four runaways without observed bow shocks. Ten of the 16 bow shocks are well aligned with the proper motion of the runaway. The aligned and misaligned bow shocks found in the mid-infrared images around the runaway or walkaway stars suggest either supersonic velocities of stars with strong stellar winds relative to the local ISM or the presence of large-scale motions within the ISM.

Acknowledgements. We thank the anonymous referee for their helpful report that improved clarity of this work. This work was partially supported by a research grant number № 21AG-1C044 from Higher Education and Science Committee of Ministry of Education, Science, Culture and Sport RA. This work presents results from the European Space Agency (ESA) space mission Gaia. Gaia data are being processed by the Gaia Data Processing and Analysis Consortium (DPAC). Funding for the DPAC is provided by national institutions, in particular the institutions participating in the Gaia MultiLateral Agreement (MLA). This publication also makes use of data products from the Wide-field Infrared Survey Explorer, which is a joint project of the University of California, Los Angeles, and the Jet Propulsion Laboratory/California Institute of Technology, funded by the National Aeronautics and Space Administration.

References

Aldoretta, E. J., Caballero-Nieves, S. M., Gies, D. R., et al. 2015, AJ, 149, 26
Andersson, E. P., Agertz, O., & Renaud, F. 2020, MNRAS, 494, 3328
Ankay, A., Kaper, L., de Bruijne, J. H. J., et al. 2001, A&A, 370, 170
Armstrong, J. J., Wright, N. J., Jeffries, R. D., Jackson, R. J., & Cantat-Gaudin, T. 2022, MNRAS, 517, 5704
Bailer-Jones, C. A. L., Rybizki, J., Fouesneau, M., Demleitner, M., & Andrae, R. 2021, AJ, 161, 147
Baranov, V. B., Krasnobaev, K. V., & Kulikovskii, A. G. 1971, Sov. Phys. Doklady, 15, 791
Bassino, L. P., Dessaunet, V. H., Muzzio, J. C., & Waldhausen, S. 1982, MNRAS, 201, 885
Benaglia, P., Romero, G. E., Martí, J., Peri, C. S., & Araudo, A. T. 2010, A&A, 517, L10
Bik, A., Puga, E., Waters, L. B. F. M., et al. 2010, ApJ, 713, 883
Binney, J., & Merrifield, M. 1998, Galactic Astronomy (Princeton: Princeton University Press)
Binney, J., & Tremaine, S. 2008, Galactic Dynamics: Second Edition (Princeton: Princeton University Press)
Blaauw, A. 1961, Bull. Astron. Inst. Netherlands, 15, 265
Blaauw, A. 1993, ASP Conf. Ser., 35, 207
Bodensteiner, J., Baade, D., Greiner, J., & Langer, N. 2018, A&A, 618, A110
Boersma, J. 1961, Bull. Astron. Inst. Netherlands, 15, 291
Borisov, S. B., Chilingarian, I. V., Rubtsov, E. V., et al. 2023, ApJS, 266, 11
Boubert, D., & Evans, N. W. 2018, MNRAS, 477, 5261
Boubert, D., Fraser, M., Evans, N. W., Green, D. A., & Izzard, R. G. 2017, A&A, 606, A14
Bressan, A., Marigo, P., Girardi, L., et al. 2012, MNRAS, 427, 127
Brown, A. G. A., Blaauw, A., Hoogerwerf, R., de Bruijne, J. H. J., & de Zeeuw, P. T. 1999, ASI Ser. C, 540, 411
Cantat-Gaudin, T., & Anders, F. 2020, A&A, 633, A99
Carey, S. J., Noriega-Crespo, A., Mizuno, D. R., et al. 2009, PASP, 121, 76
Carretero-Castrillo, M., Ribó, M., & Paredes, J. M. 2023, A&A, 679, A109
Carretero-Castrillo, M., Benaglia, P., Paredes, J. M., & Ribó, M. 2025, A&A, 694, A250
Comeron, F., & Kaper, L. 1998, A&A, 338, 273
Comeron, F., Torra, J., & Gomez, A. E. 1998, A&A, 330, 975
Corti, M., Bosch, G., & Niemela, V. 2007, A&A, 467, 137
Crampton, D. 1972, MNRAS, 158, 85
D'Amico, N., Stappers, B. W., Bailes, M., et al. 1998, MNRAS, 297, 28
de Wit, W. J., Testi, L., Palla, F., & Zinnecker, H. 2005, A&A, 437, 247
Denoyelle, J. 1977, A&AS, 27, 343
Dinçel, B., Paylı, G., Yerli, S. K., et al. 2026, A&A, 707, A50
Dorigo Jones, J., Oey, M. S., Paggeot, K., Castro, N., & Moe, M. 2020, ApJ, 903, 43
Drew, J. E., Monguió, M., & Wright, N. J. 2021, MNRAS, 508, 4952
Eggen, O. J. 1982, ApJS, 50, 199
Eldridge, J. J., Langer, N., & Tout, C. A. 2011, MNRAS, 414, 3501
Elia, D., Massi, F., Strafella, F., et al. 2007, ApJ, 655, 316
Ellerbroek, L. E., Bik, A., Kaper, L., et al. 2013, A&A, 558, A102
Evans, D. S. 1967, IAU Symp., 30, 57
Fazio, G. G., Hora, J. L., Allen, L. E., et al. 2004, ApJS, 154, 10
Feast, M. W., Stoy, R. H., Thackeray, A. D., & Wesselink, A. J. 1961, MNRAS, 122, 239
Fitzgerald, M. P., Luiken, M., Maitzen, H. M., & Moffat, A. F. J. 1979, A&AS, 37, 345
Fortin, F., García, F., & Chaty, S. 2022, A&A, 665, A69
Fortin, F., García, F., Simaz Bunzel, A., & Chaty, S. 2023, A&A, 671, A149
Froebrich, D., Scholz, A., & Raftery, C. L. 2007, MNRAS, 374, 399
Fujii, M. S., & Portegies Zwart, S. 2011, Science, 334, 1380
Gaia Collaboration. 2022, VizieR Online Data Catalog: I/355
Gaia Collaboration (Brown, A. G. A., et al.) 2021, A&A, 649, A1
Gaia Collaboration (Drimmel, R., et al.) 2023, A&A, 674, A37
Gamen, R., Barbà, R. H., Walborn, N. R., et al. 2015, A&A, 583, L4
Garrison, R. F., Hiltner, W. A., & Schild, R. E. 1977, ApJS, 35, 111
Gies, D. R. 1987, ApJS, 64, 545
Giménez-García, A., Shenar, T., Torrejón, J. M., et al. 2016, A&A, 591, A26
Gontcharov, G. A. 2006, Astron. Lett., 32, 759
Gualandris, A., Portegies Zwart, S., & Eggleton, P. P. 2004, MNRAS, 350, 615
Guarcello, M. G., Almendros-Abad, V., Lovell, J. B., et al. 2025, A&A, 693, A120
Gvaramadze, V. V. 2009, MNRAS, 395, L85
Gvaramadze, V. V., & Bomans, D. J. 2008, A&A, 490, 1071
Gvaramadze, V. V., Kroupa, P., & Pflamm-Altenburg, J. 2010, A&A, 519, A33
Gvaramadze, V. V., Kniazev, A. Y., Kroupa, P., & Oh, S. 2011, A&A, 535, A29
Gvaramadze, V. V., Weidner, C., Kroupa, P., & Pflamm-Altenburg, J. 2012, MNRAS, 424, 3037
Gvaramadze, V. V., Menten, K. M., Kniazev, A. Y., et al. 2014, MNRAS, 437, 843
Gvaramadze, V. V., Alexashov, D. B., Katushkina, O. A., & Kniazev, A. Y. 2018, MNRAS, 474, 4421
Helou, G., & Walker, D. W. 1988, in Infrared Astronomical Satellite (IRAS) Catalogs and Atlases (USA: NASA), 7
Henney, W. J., & Arthur, S. J. 2019, MNRAS, 489, 2142
Hohle, M. M., Neuhäuser, R., & Schutz, B. F. 2010, Astron. Nachr., 331, 349
Holgado, G., Simón-Díaz, S., Barbá, R. H., et al. 2018, A&A, 613, A65
Hoogerwerf, R., de Bruijne, J. H. J., & de Zeeuw, P. T. 2000, ApJ, 544, L133
Houk, N. 1978, Michigan Catalogue of Two-dimensional Spectral Types for the HD Stars (Ann Arbor : Dept. of Astronomy, University of Michigan)
Howarth, I. D., & Prinja, R. K. 1989, ApJS, 69, 527
Humphreys, R. M. 1978, ApJS, 38, 309
Huthoff, F., & Kaper, L. 2002, A&A, 383, 999
Iping, R., Sonneborn, G., & Kaper, L. 2007, AAS Meeting Abstracts, 210, 19.10
Johnson, D. R. H., & Soderblom, D. R. 1987, AJ, 93, 864
Kaper, L. 2000, ASP Conf. Ser., 204, 3
Kaper, L., van Loon, J. T., Augusteijn, T., et al. 1997, ApJ, 475, L37
Katz, D., Sartoretti, P., Guerrier, A., et al. 2023, A&A, 674, A5
Kharchenko, N. V., Scholz, R. D., Piskunov, A. E., Röser, S., & Schilbach, E. 2007, Astron. Nachr., 328, 889

Kharchenko, N. V., Piskunov, A. E., Schilbach, E., Röser, S., & Scholz, R. D. 2013, A&A, 558, A53
Kilkenny, D. 1993, South African Astron. Observ. Circ., 15, 53
Klare, G., & Neckel, T. 1977, A&AS, 27, 215
Kobulnicky, H. A., Chick, W. T., Schurhammer, D. P., et al. 2016, ApJS, 227, 18
Kobulnicky, H. A., Chick, W. T., & Povich, M. S. 2019, AJ, 158, 73
Krishnakumar, M. A., Mitra, D., Naidu, A., Joshi, B. C., & Manoharan, P. K. 2015, ApJ, 804, 23
Krone-Martins, A., & Moitinho, A. 2014, A&A, 561, A57
Krtička, J. 2014, A&A, 564, A70
Kudritzki, R.-P., & Puls, J. 2000, ARA&A, 38, 613
Lequeux, J. 2005, The Interstellar Medium (Berlin: Springer)
Lindegren, L., Bastian, U., Biermann, M., et al. 2021, A&A, 649, A4
MacConnell, D. J., & Bidelman, W. P. 1976, AJ, 81, 225
Mackey, J. 2023, IAU Symp., 370, 205
Magakian, T. Y. 2003, A&A, 399, 141
Maíz Apellániz, J. 2013, in Highlights of Spanish Astrophysics VII, eds. J. C. Guirado, L. M. Lara, V. Quilis, & J. Gorgas (Spain: Spanish Astronomical Society), 657
Maíz Apellániz, J., Pantaleoni González, M., Barbá, R. H., et al. 2018, A&A, 616, A149
Maíz Apellániz, J., Barbá, R. H., Fernández Aranda, R., et al. 2022, A&A, 657, A131
Marigo, P., Bressan, A., Nanni, A., Girardi, L., & Pumo, M. L. 2013, MNRAS, 434, 488
Marigo, P., Girardi, L., Bressan, A., et al. 2017, ApJ, 835, 77
Massi, F., Di Carlo, E., Codella, C., et al. 2010, A&A, 516, A52
Mel'nik, A. M., & Dambis, A. K. 2017, MNRAS, 472, 3887
Meyer, D. M. A., Mackey, J., Langer, N., et al. 2014, MNRAS, 444, 2754
Mirabel, I. F., & Rodrigues, I. 2003, Science, 300, 1119
Mokiem, M. R., de Koter, A., Vink, J. S., et al. 2007, A&A, 473, 603
Moutzouri, M., Mackey, J., Castro, N., et al. 2025, A&A, 704, A268
Muzzio, J. C., & Orsatti, A. M. 1977, AJ, 82, 474
Nesterov, V. V., Kuzmin, A. V., Ashimbaeva, N. T., et al. 1995, A&AS, 110, 367
Neuhäuser, R., Gießler, F., & Hambaryan, V. V. 2020, MNRAS, 498, 899
Nguyen, C. T., Costa, G., Girardi, L., et al. 2022, A&A, 665, A126
Panagia, N. 1973, AJ, 78, 929
Pantaleoni González, M., Maíz Apellániz, J., Barbá, R. H., et al. 2025, MNRAS, 543, 63
Parthasarathy, M., Drilling, J. S., Vijapurkar, J., & Takeda, Y. 2012, PASJ, 64, 57
Pastorelli, G., Marigo, P., Girardi, L., et al. 2019, MNRAS, 485, 5666
Pastorelli, G., Marigo, P., Girardi, L., et al. 2020, MNRAS, 498, 3283
Patten, N., Kobulnicky, H. A., Povich, M. S., et al. 2025, ApJ, 988, 183
Pera, M. S., Perren, G. I., Moitinho, A., Navone, H. D., & Vazquez, R. A. 2021, A&A, 650, A109
Peri, C. S., Benaglia, P., Brookes, D. P., Stevens, I. R., & Isequilla, N. L. 2012, A&A, 538, A108
Pflamm-Altenburg, J., & Kroupa, P. 2010, MNRAS, 404, 1564
Poggio, E., Drimmel, R., Cantat-Gaudin, T., et al. 2021, A&A, 651, A104
Pössel, M. 2020, Open J. Astrophys., 3, 2
Pourbaix, D., Tokovinin, A. A., Batten, A. H., et al. 2004, A&A, 424, 727
Poveda, A., Ruiz, J., & Allen, C. 1967, Boletin de los Observatorios Tonantzintla y Tacubaya, 4, 86
Povich, M. S., Benjamin, R. A., Whitney, B. A., et al. 2008, ApJ, 689, 242
Prinja, R. K., Barlow, M. J., & Howarth, I. D. 1990, ApJ, 361, 607
Prisinzano, L., Damiani, F., Guarcello, M. G., et al. 2018, A&A, 617, A63
Rao, A., Gandhi, P., Knigge, C., et al. 2020, MNRAS, 495, 1491
Reed, B. C. 2000, AJ, 119, 1855
Reed, B. C. 2003, AJ, 125, 2531
Reid, M. J., & Brunthaler, A. 2004, ApJ, 616, 872
Reid, M. J., Menten, K. M., Brunthaler, A., et al. 2019, ApJ, 885, 131
Renzo, M., Zapartas, E., de Mink, S. E., et al. 2019, A&A, 624, A66
Romani, R. W., Kerr, M., Craig, H. A., et al. 2011, ApJ, 738, 114
Rosenfield, P., Marigo, P., Girardi, L., et al. 2016, ApJ, 822, 73
Sahu, M. S. 1992, PhD thesis, Kapteyn Institute, Postbus 800 9700 AV Groningen, The Netherlands
Song, F., Esamdin, A., Hu, Q., & Zhang, M. 2022, A&A, 666, A75
Sota, A., Maíz Apellániz, J., Morrell, N. I., et al. 2014, ApJS, 211, 10
Stoop, M. 2024, PhD thesis, Anton Pannekoek Institute for Astronomy, University of Amsterdam, The Netherlands
Stoop, M., Kaper, L., de Koter, A., et al. 2023, A&A, 670, A108
Stoop, M., de Koter, A., Kaper, L., et al. 2024a, Nature, 634, 809
Stoop, M., Derkink, A., Kaper, L., et al. 2024b, A&A, 681, A21
Strömgren, B. 1939, ApJ, 89, 526
Tarricq, Y., Soubiran, C., Casamiquela, L., et al. 2021, A&A, 647, A19
van Buren, D., & McCray, R. 1988, ApJ, 329, L93
van Buren, D., Noriega-Crespo, A., & Dgani, R. 1995, AJ, 110, 2914
van den Bergh, S., & Herbst, W. 1975, AJ, 80, 208
van den Eijnden, J., Heywood, I., Fender, R., et al. 2022, MNRAS, 510, 515
van den Heuvel, E. P. J., Portegies Zwart, S. F., Bhattacharya, D., & Kaper, L. 2000, A&A, 364, 563
van der Meij, V., Guo, D., Kaper, L., & Renzo, M. 2021, A&A, 655, A31
van Rensbergen, W., Vanbeveren, D., & De Loore, C. 1996, A&A, 305, 825
Vijapurkar, J., & Drilling, J. S. 1993, ApJS, 89, 293
Wilkin, F. P. 2000, ApJ, 532, 400
Williams, S. J., Gies, D. R., Hillwig, T. C., McSwain, M. V., & Huang, W. 2011, AJ, 142, 146
Wilson, R. E. 1953, in General catalogue of stellar radial velocities, Carnegie Institute Washington D.C. Publication, 0
Wright, E. L., Eisenhardt, P. R. M., Mainzer, A. K., et al. 2010, AJ, 140, 1868

Appendix A: Members of Vel OB1 collected from literature, runaways, and parent clusters

This section presents supporting material related to the identification of candidate members of the Vel OB1 association and the characterisation of associated OB runaway stars. Table A.1 lists the candidate Vel OB1 members compiled from the literature together with their *Gaia* DR3 astrometric parameters.

Figure A.1 provides an overview of the parallax distribution of *Gaia* DR3 sources in the Vel OB1 region and the spatial distribution of young stellar over-densities in Galactic coordinates, placing the candidate members, clusters, and runaway stars in their distance and spatial context. Figure A.2 further illustrates the distance and proper-motion distributions of the candidate members and runaways, and compares them with the mean kinematics of Vel OB1 and the young clusters.

The astrometric and kinematic properties of the OB runaway stars are summarised in Table A.2, while Table A.3 presents estimates of their kinematical ages and, where possible, their likely parent clusters, distinguishing confirmed from candidate runaways.

Appendix B: Membership, distance, and age of young stellar clusters in Vel OB1 based on *Gaia* DR3

In this section we provide the figures used for the analysis of the membership, distance and age of the six young stellar clusters studied in Vel OB1. In Fig. B.1, we show the parallax distribution of the members of each cluster against their G-magnitude. The best-fit distance corresponds to the maximum of the log-likelihood function. The 16^{th} and 84^{th} percentiles of the distance distribution derived from the likelihood function provide the 1σ-uncertainty range. The best-fit parallax and the 1σ uncertainties on the parallax range of each cluster are shown with the red solid and grey dashed lines in each panel of Fig. B.1, respectively.

The distribution on the sky of the members of each young cluster is shown in Fig. B.2 in Galactic coordinates. Members and field stars are in blue and grey, respectively. The median value of the coordinates of the clusters are taken as the centre of each panel.

Figure B.3 presents colour-absolute magnitude diagrams for the individual young clusters contained in Vel OB1 based on the *Gaia* membership analysis; cluster members are represented by the blue dots (including error bars). We estimated the mean reddening of the cluster based on a near-infrared colour-colour diagram of the 2MASS counterparts of the *Gaia* DR3 members and took this value to obtain the best-fit isochrone. The mean reddening A_V and best age are indicated in the legend of each figure. The extinction in the Vel OB1 region varies strongly; in Tab. 1 we provide the range measured in the near-infrared colour-colour diagram for each cluster. For comparison, in each panel we plot isochrones corresponding to a minimum (red curve) and maximum (green curve) age based on the 100 iterations for each cluster.

Appendix C: AllWISE images OB runaways with no evidence of wind bow shock

We explored the AllWISE survey in the vicinity of all OB runaway stars associated with Vel OB1 to search for arc-like structures. Figure C.1 presents AllWISE colour-composite images of 18 OB runaway stars in Vel OB1. Although in some cases (e.g. HD 75991, HD 71649, HD 78927) emission features are present close to the stars and could be related to their stellar winds, the available data are insufficient to draw firm conclusions.

Appendix D: Notes on individual objects

HD 75222 is a B0 Ia supergiant compiled in the list of Reed (2000) (Tab. A.1) and identified as an OB runaway star based on its 2D peculiar velocity of 72 km s^{-1}, in agreement with the findings of Carretero-Castrillo et al. (2023). It is moving away from us with a radial velocity of 64 km s^{-1} at its current distance of 2017 pc and height above the plane of 147 pc. When reconstructing its projected path on the sky, one obtains a match with the young open cluster Bochum 7 ($d \simeq 2000$ pc, age $\sim$ 27 Myr, Song et al. 2022; Gaia Collaboration 2023) 5.5 Myr ago.

CD-41 4637 is a massive binary with an unresolved companion (Aldoretta et al. 2015) and is not included in the list of Reed (2000) (Tab. A.1). The spectral type of the brightest component is O6 Ib(f)(n) (Vijapurkar & Drilling 1993) and its current distance is 2280 pc (Bailer-Jones et al. 2021) at a height of 92 pc above the Galactic plane. The AllWISE colour-composite image (Fig. 4) presents a bow shock aligned with the runaway velocity of CD-41 4637 confirming its supersonic motion. Aldoretta et al. (2015) suggest that CD-41 4637 is not associated with any cluster or association, that it is not a runaway star, and that its distance is 3.7 kpc. The peculiar transverse velocity of CD-41 4637 star (V_{pec}=35 km s^{-1}), however, demonstrates its runaway nature. Denoyelle (1977) included CD-41 4637 in their list of young stars with $A_v = 3.25$ mag and obtained a distance of 2.09 kpc. Kilkenny (1993) and Klare & Neckel (1977) estimated a distance of 2.3 kpc and 2.66 kpc, respectively, in good agreement with the distance based on the *Gaia* parallax.

The path of CD-41 4637 suggests that it escaped from RCW 34 about 2 Myr ago. The estimated age range of the RCW 34 H II region and cluster is 4.7 – 9.9 Myr (Tab. 1), consistent with the kinematic age of CD-41 4637 suggesting a dynamical ejection origin of the young binary (Denoyelle 1977). Bik et al. (2010) mention that the central star (vdBH 25a, van den Bergh & Herbst 1975) of the H II region might not have created an associated bubble since it is near the northern edge. Possibly the runaway O supergiant CD-41 4637 has contributed to the formation of this bubble since it moved away from the cluster (but see 6.4).

HD 75860 is a B1.5 Iabp blue supergiant with a mass of 15.5 $M_\odot$ (Hohle et al. 2010) and a peculiar velocity of 31 km s^{-1}. Denoyelle (1977) included the star in their list of young stars ($A_v = 2.67$ mag) and obtained a distance of 1.7 kpc. The *Gaia* distance is $2.27^{+0.20}_{-0.23}$ kpc (Bailer-Jones et al. 2021). The AllWISE colour-composite image (Fig. 4) shows the aligned bow shock. HD 75860 is currently located in the Gum 18 H II region. Therefore, the determined Strömgren radius (Tab. 2) may be spurious and the extraction of the extended H II region created by UV emission of only HD 75860 is challenging. The observed bow shock is one of three arc-like molecular structures in Gum 18 H II region (Elia et al. 2007). The path of HD 75860 matches with an origin in the [KPS2012] MWSC 1594 (indicated as Cl 1594 in this work) open cluster 1.2 Myr ago. The parameters of the cluster: distance 1.9 kpc, age $\sim$ 130 Myr, and μ^*_α of -4.94 mas yr^{-1} and μ_δ of 6.18 mas yr^{-1} (Kharchenko et al. 2013) differ from our results (see Tab. 1). Froebrich et al. (2007) identified 579 stars in the cluster; we found only 21 members and arrive at a distance of $2.084^{+0.043}_{-0.041}$ kpc. Thus, the Cl 1594 cluster and HD 75860 are located at the same distance. From the age range of Cl 1594

Table A.1. Candidate members of Vel OB1 according to literature.

Star	l	b	Sp. Type	V_r	Parallax	μ_{l^*}	μ_b	G	D	V_{pec}		Member	Ref (SpT,V_r)
										LSR	Vel OB1		
–	(deg)	(deg)	–	(km s^{-1})	(mas)	(mas yr^{-1})	(mas yr^{-1})	(mag)	(pc)	(km s^{-1})	(km s^{-1})	–	–
(1)	(2)	(3)	(4)	(5)	(6)	(7)	(8)	(9)	(10)	(11)	(12)	(13)	(14)
HD 71649**	255.76	1.00	B1 IIIn	–	0.44 ± 0.02	-8.47 ± 0.02	0.05 ± 0.02	8.7	2256	39.6	36.8	N,R	9
CD-38 4168**	256.13	-2.88	O8.5 III	–	0.50 ± 0.02	-5.15 ± 0.02	-0.25 ± 0.02	9.1	1986	3.7	15.9	N?	9
HD 75222**	258.29	4.18	B0 Ia	64	0.49 ± 0.02	-11.51 ± 0.02	3.10 ± 0.02	7.3	2017	*74.6*	*78.8*	N,R	9 / 18
HD 69882**	259.50	-3.91	B0.7 Ib	25.9	0.70 ± 0.02	-6.93 ± 0.02	-1.04 ± 0.02	7.1	1427	*9.3*	*10.9*	Y	9 / 19
HD 71528**	260.13	-2.33	B1.5 III	–	0.76 ± 0.04	-6.85 ± 0.04	-1.22 ± 0.05	7.8	1331	5.9	17.1	Y?	9
HD 70583**	260.78	-3.96	B9 Ia	–	0.47 ± 0.02	-6.45 ± 0.02	-0.92 ± 0.02	7.8	2149	9.0	8.5	Y	9
HD 70122**	261.07	-4.71	B1 II	–	0.48 ± 0.01	-6.22 ± 0.01	-1.34 ± 0.01	9.1	2094	9.4	5.9	Y	9
HD 71609**	261.20	-3.01	B3 II	25	0.66 ± 0.02	-7.26 ± 0.02	-1.15 ± 0.02	7.8	1501	*10.4*	*6.8*	Y?	9 / 2
HD 71304**	261.76	-3.77	O9 II	25	0.48 ± 0.02	-6.48 ± 0.02	-1.22 ± 0.02	8.1	2096	*14.2*	*8.1*	Y	3 / 16,2
HD 72576**	262.09	-2.48	B2 II/III	–	0.84 ± 0.02	-7.25 ± 0.02	-1.46 ± 0.02	8.2	1190	5.3	18.3	N	9
CD-43 4488**	262.53	-1.46	O9/B0	–	0.56 ± 0.01	-6.93 ± 0.01	-1.55 ± 0.02	10.4	1792	9.1	3.0	Y	5
HD 75759*	262.80	1.25	O9 Vn	23.4	1.08 ± 0.04	-6.23 ± 0.04	-2.15 ± 0.05	6.0	934	*5.0*	*30.2*	N	–
HD 73420**	262.81	-1.95	B0 III	–	0.55 ± 0.02	-7.24 ± 0.02	-1.14 ± 0.02	8.8	1819	9.9	4.9	Y	9
HD 77581**	263.06	3.93	B0.5 Ia	-3.2	0.51 ± 0.02	-10.15 ± 0.02	2.51 ± 0.02	6.7	1960	*64.7*	*60*	N,R,B	22/19
HD 76341**	263.53	1.52	O9.2 IV	26	0.90 ± 0.05	-5.91 ± 0.05	-1.48 ± 0.05	7.0	1137	*5.3*	*27.3*	N	3 / 14
CD-42 4694**	263.61	0.55	O9 V	–	0.41 ± 0.03	-6.97 ± 0.03	-1.41 ± 0.03	10.4	2466	13.4	22.4	Y?,R?,B?	10
HD 73568*	263.80	-2.50	B0.5 III	–	0.50 ± 0.03	-5.87 ± 0.03	-0.57 ± 0.04	8.3	2023	2.9	7.2	Y	1,4
HD 72554**	263.94	-3.86	B1.5 Ib	–	0.51 ± 0.02	-7.05 ± 0.02	-1.34 ± 0.02	8.1	1984	10.9	7.2	Y	9
HD 75211*	263.96	-0.47	O9 Ib	20	0.64 ± 0.02	-10.01 ± 0.02	-1.79 ± 0.02	7.4	1550	*30.4*	*17.1*	N,R?	–
HD 74194*	264.04	-1.95	O8.5 Ib	-2.7	0.45 ± 0.02	-9.40 ± 0.02	-2.18 ± 0.02	7.5	2220	*54.4*	*51.3*	N,R	1
CD-42 4819**	264.13	1.90	B2 Vp	–	1.24 ± 0.03	-7.38 ± 0.02	-2.96 ± 0.02	9.6	808	3.7	29.9	N	23
HD 75860*	264.14	0.27	B1.5 Iabp	16.8	0.45 ± 0.04	-7.94 ± 0.04	-2.11 ± 0.05	7.3	2276	*31.1*	*28.7*	Y?,R,B	9
CD-44 4691*	264.26	-2.02	B2.5 II	39	0.47 ± 0.02	-6.55 ± 0.02	-1.09 ± 0.02	8.4	2121	*8.5*	*15.1*	Y	1 / 1
HD 74371*	264.44	-2.01	B5 Iab/b	24.6	0.61 ± 0.07	-7.10 ± 0.07	-1.81 ± 0.07	5.1	1787	*11.6*	*4.5*	Y	/ 1
HD 76031**	264.50	0.30	B0.5 IV	–	0.57 ± 0.02	-7.02 ± 0.03	-2.15 ± 0.03	8.8	1752	11.3	6.1	Y,R,B	9
HD 73658**	264.68	-3.13	B1 II	52	0.57 ± 0.02	-7.28 ± 0.03	-1.43 ± 0.02	6.8	1783	*22.8*	*26.3*	Y,R	9 / 14
CD-44 4865*	264.69	-0.37	O9.5 Ib	39	0.51 ± 0.03	-7.81 ± 0.03	-0.33 ± 0.03	9.2	1937	*14.6*	*21.6*	R	1
HD 73919**	264.78	-2.90	B1 V	–	0.61 ± 0.01	-7.24 ± 0.02	-1.33 ± 0.02	8.8	1656	7.6	2.9	Y	9
CD-45 4355**	264.80	-2.91	B1 Vne	–	0.60 ± 0.01	-7.63 ± 0.01	-1.48 ± 0.02	9.3	1671	11.0	1.7	Y	12
CD-45 4394**	264.87	-2.58	B2 Vne	78	0.55 ± 0.01	-6.91 ± 0.01	-1.09 ± 0.01	10.0	1826	*46.4*	*52.5*	N?,R	11 / 21
HD 74677*	265.17	-2.20	B2 II	23	0.49 ± 0.01	-5.94 ± 0.02	-1.09 ± 0.02	8.6	2063	*12.3*	*2.2*	Y	4/17
CD-45 4447**	265.18	-2.26	O7.5 V	–	1.53 ± 0.39	-5.85 ± 0.45	0.07 ± 0.45	10.9	888	10.5	42.3	N,R?,B?	8
HD 74180*	265.28	-2.95	F2 Ia	31	0.43 ± 0.10	-7.28 ± 0.11	-2.12 ± 0.12	3.6	2532	*22.3*	*25.5*	Y?,R	4/24
HD 74920**	265.29	-1.95	O7.5 IVn((f))	–	0.57 ± 0.03	-12.35 ± 0.03	-0.66 ± 0.03	7.5	1753	49.6	44.5	N,R	3
HD 75149*	265.33	-1.69	B3 Ia	25.2	0.70 ± 0.05	-6.57 ± 0.06	-0.93 ± 0.06	5.3	1465	*3.3*	*15.2*	Y	/ 1
CD-45 4606*	265.44	-0.94	B0.5 V	6	0.46 ± 0.01	-7.11 ± 0.01	-0.75 ± 0.01	8.9	2149	*29.7*	*23.9*	Y,R	1
HD 75276*	265.61	-1.73	F2 lab	32	0.70 ± 0.04	-6.61 ± 0.04	-0.91 ± 0.04	5.6	1443	*4.3*	*16.8*	Y?	–
CD-45 4635*	265.67	-0.90	B0.5 III	18	0.45 ± 0.01	-7.09 ± 0.02	-0.66 ± 0.02	8.9	2235	*19.2*	*17.6*	Y,R	1 / 1
HD 74711**	265.73	-2.61	B1 III	–	0.79 ± 0.02	-10.38 ± 0.02	-2.46 ± 0.03	7.1	1272	23.1	4.7	N,R?	9
HD 75309**	265.90	-1.90	B1 IIp	–	0.55 ± 0.04	-6.96 ± 0.05	-0.99 ± 0.04	7.8	1931	5.0	3.5	Y	9
HD 78927**	266.02	3.10	B1 II/III	27	0.46 ± 0.02	-6.88 ± 0.02	0.36 ± 0.02	8.2	2169	*16.5*	*21.1*	Y,R	4 / 2
CD-45 4676*	266.18	-0.85	B0.5 III	28	0.54 ± 0.01	-7.03 ± 0.02	-0.89 ± 0.02	8.8	1875	*6.3*	*6.3*	Y	–
HD 74401**	266.23	-3.38	B1.5 IIIne	–	0.57 ± 0.01	-7.34 ± 0.02	-1.16 ± 0.02	8.9	1762	8.0	3.3	Y	9
CD-45 4719**	266.46	-0.31	B0	–	0.47 ± 0.01	-7.10 ± 0.01	-0.64 ± 0.02	9.6	2134	7.6	14.1	Y	5
HD 78958**	266.47	2.73	B0/1 Iab	35	0.47 ± 0.01	-6.03 ± 0.01	-0.70 ± 0.01	8.8	2133	*4.7*	*13.8*	Y,R?,B?	4 / 14
HD 75658**	266.87	-2.29	B1 IVe	–	0.65 ± 0.02	-8.12 ± 0.02	-2.07 ± 0.02	8.0	1536	13.4	3.6	N?	9
HD 75534**	267.01	-2.56	B1 Ib	–	0.53 ± 0.02	-6.66 ± 0.02	-1.51 ± 0.02	7.7	1876	7.5	2.6	Y	9
CD-45 4826**	267.13	0.80	O9	–	0.47 ± 0.01	-7.05 ± 0.01	-0.72 ± 0.01	9.9	2143	8.0	16.4	Y	2
HD 75991**	267.17	-2.07	B0.5 III	9	0.62 ± 0.01	-7.31 ± 0.02	-1.00 ± 0.02	8.9	1618	*19.9*	*14.9*	Y,R	9 / 2
CD-46 4786*	267.35	-1.03	B0.5 Ib	23	0.47 ± 0.01	-6.79 ± 0.02	-0.96 ± 0.01	8.7	2132	*9.3*	*9.1*	RCW38	1,6
HD 79186**	267.36	2.25	B5 Ia	28	0.61 ± 0.07	-7.05 ± 0.07	-1.17 ± 0.08	4.9	1811	*3.0*	*8.7*	Y	4 / 14
CD-47 4490*	267.40	-1.67	Bl III	–	0.54 ± 0.01	-6.71 ± 0.01	-0.66 ± 0.02	9.5	1844	1.7	6.5	Y	1,7
HD 76535**	267.42	-1.52	O9	25	0.47 ± 0.02	-7.01 ± 0.02	-0.98 ± 0.02	8.5	2174	*9.1*	*11.4*	RCW38	4 / 20
HD 76556*	267.58	-1.63	O6 IV(n)((f))p	28.2	0.55 ± 0.03	-6.91 ± 0.03	-1.36 ± 0.04	8.0	1820	*7.0*	*5.7*	Y	3 / 15
CD-45 4820**	267.59	0.31	OB	–	0.50 ± 0.01	-6.94 ± 0.02	-0.33 ± 0.02	11.1	2013	6.9	13.4	Y	2
CD-47 4551**	267.98	-1.36	O5 Ifc	136	0.59 ± 0.03	-6.82 ± 0.03	-1.12 ± 0.03	8.0	1697	*107.0*	*114.1*	R	2/25
HD 80057**	267.99	2.87	A0 Iab	25.7	0.56 ± 0.02	-7.31 ± 0.02	-0.07 ± 0.03	5.9	1798	*12.6*	*13.5*	Y	4 / 14
CD-47 4550**	268.00	-1.38	O7 V((f))z	–	0.56 ± 0.01	-6.74 ± 0.01	-1.13 ± 0.01	9.9	1789	2.6	4.0	RCW38	3
CD-47 4564**	268.46	-1.65	B0.5 III	-2.00	0.59 ± 0.02	-6.39 ± 0.02	-1.76 ± 0.02	9.5	1718	*31.4*	*25.3*	R,B	7 / 17
HD 78344**	268.89	-0.38	O9.5/B0 (Ib)	-5.70	0.46 ± 0.02	-5.98 ± 0.02	-2.29 ± 0.02	8.5	2169	*42.0*	*29.1*	R	4 / 2
HD 77207**	268.96	-1.90	B7 Iab+	–	0.56 ± 0.02	-6.29 ± 0.02	-1.64 ± 0.02	9.2	1784	7.8	6.8	Y,R,B	4
HD 77852**	269.15	-1.20	B8/9 Iab/b	–	0.57 ± 0.02	-7.03 ± 0.02	-0.64 ± 0.02	8.3	1747	3.1	7.8	Y	4
CPD-47 3051**	269.21	-0.91	B0 V	–	0.49 ± 0.02	-6.86 ± 0.02	-0.37 ± 0.02	10.8	2069	4.1	12.2	Y,R,B	26
HD 76968**	270.22	-3.37	O9.2 Ib	-22	0.46 ± 0.02	-1.62 ± 0.02	-1.25 ± 0.02	7.0	2199	*74.3*	*60.9*	N,R	3 / 16
HD 82830**	271.43	3.62	B0/2 Ie	–	0.51 ± 0.01	-6.87 ± 0.02	-1.75 ± 0.01	9.1	1968	6.1	10.5	Y	4
CD-48 4654**	271.90	0.70	B2 Ib	–	0.47 ± 0.01	-7.27 ± 0.02	-0.80 ± 0.01	9.7	2325	4.6	17.2	Y	7
HD 297433**	272.07	0.44	O8/9	–	0.43 ± 0.01	-6.52 ± 0.01	-0.27 ± 0.01	8.9	2323	5.9	17.9	Y	5
HD 298298**	272.73	-3.31	B0	–	0.64 ± 0.01	-6.35 ± 0.01	-1.04 ± 0.02	9.0	1559	6.9	14.0	Y	13
HD 80558**	273.07	-1.47	B6 Ia	21.7	0.54 ± 0.03	-7.03 ± 0.03	-1.19 ± 0.03	5.7	1862	*4.7*	*5.2*	Y	4 / 18
HD 84136**	273.72	3.19	B1/2 II	–	0.38 ± 0.01	-5.68 ± 0.01	-0.40 ± 0.01	8.7	2634	12.6	17.3	Y	4
HD 81471**	273.78	-1.01	A5 Ia/ab	28	0.32 ± 0.02	-6.41 ± 0.03	-0.80 ± 0.03	5.9	3060	*6.5*	*35.4*	N	4 / 17
HD 298425**	274.34	0.04	O9 V	10	0.56 ± 0.01	-6.91 ± 0.01	-0.84 ± 0.01	9.6	1782	*13.4*	*7.9*	Y	11 / 17
HD 85356**	274.37	4.60	B2Ib	–	0.57 ± 0.03	-4.05 ± 0.04	-0.29 ± 0.03	8.0	1754	27.4	27.7	N?,R	2
HD 81370**	274.41	-1.81	B1 (III)n	13	0.55 ± 0.02	-6.80 ± 0.02	-1.17 ± 0.02	8.7	1808	*11.0*	*4.3*	Y	4 / 17
HD 298429**	274.47	-0.25	O8.5 V	25	0.55 ± 0.01	-5.37 ± 0.01	0.24 ± 0.01	9.5	1831	*20.1*	*23.4*	Y,R	3 / 16
HD 298420**	274.58	-1.81	B1/2	–	0.41 ± 0.02	-6.37 ± 0.02	-0.62 ± 0.02	9.8	2439	4.9	19.1	Y	5
HD 298448**	274.90	-1.65	B1/3	–	0.36 ± 0.01	-6.27 ± 0.01	-0.38 ± 0.01	9.5	2733	4.5	27.6	Y?	5

References. 1. Humphreys (1978); 2. Reed (2000); 3. Sota et al. (2014); 4. Houk (1978); 5. Reed (2003); 6. MacConnell & Bidelman (1976); 7. Bassino et al. (1982); 8. Corti et al. (2007); 9. Garrison et al. (1977); 10. Vijapurkar & Drilling (1993); 11. Feast et al. (1961); 12. Fitzgerald et al. (1979); 13. Nesterov et al. (1995); 14. Gontcharov (2006); 15. Williams et al. (2011); 16. Holgado et al. (2018); 17. Evans (1967); 18. Kharchenko et al. (2007); 19. Pourbaix et al. (2004); 20. Crampton (1972); 21. Wilson (1953); 22.Maíz Apellániz et al. (2018); 23. Parthasarathy et al. (2012); 24. Borisov et al. (2023); 25. Tarricq et al. (2021); 26. Kobulnicky et al. (2019).

Notes. (1) Stellar ID, (2),(3) Galactic coordinates, (4) Spectral type, (5) Radial velocity, (6)-(9) *Gaia* DR3 corrected parallax, proper motion in Galactic coordinates and G magnitude, respectively, (10) Distance (Bailer-Jones et al. 2021), (11) Peculiar space (*italic*) or transverse velocity relative to LSR (see Section 3.1), (12) Peculiar (*italic*) or transverse velocity relative to Vel OB1 (see Section 3.1), (13) Confirmed member of Vel OB1 (or of young cluster), or runaway R, with bow shock B, (14) Reference for spectral type/radial velocity. (*)Object from Humphreys (1978), (**)Object from Reed (2000). Objects in common with the list of OB runaways in Carretero-Castrillo et al. (2023) are in bold.

(2.6−6.6 Myr), we propose that HD 75860 underwent a dynamical ejection. Exploring the region surrounding the Cl 1594 open cluster, an unknown star-forming region may be aligned with the open cluster. There are several reflection nebulae in this region (Magakian 2003). Taking into account the proper motion and age discrepancy between our results (Tab. 1) and the data known from the literature, probably the parent cluster of HD 75860 is the star-forming region (with our estimated parameters) rather than the Cl 1594 open cluster.

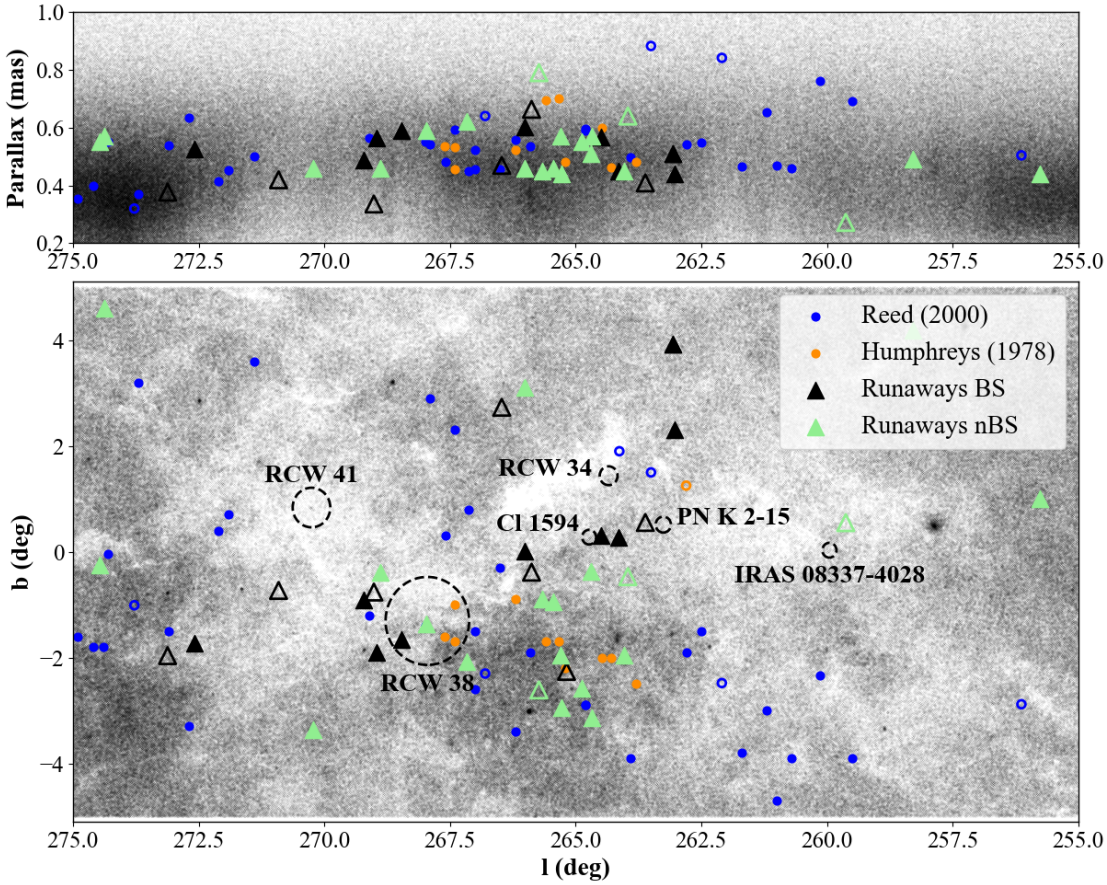

Fig. A.1. The about 2 million *Gaia* DR3 sources in the region contained by Vel OB1. The members proposed by Humphreys (1978) (orange) and Reed (2000) (blue) are indicated. Open circles refer to non-members (see Tab. A.1). The black and green triangles represent the runaways with (Runaways BS) and without (Runaways nBS) an observed bow shock. Open triangles refer to candidate runaways (see Tab. A.2). *Upper panel:* The parallax distribution as a function of Galactic longitude. *Lower panel:* The position of known young clusters in the distance range of Vel OB1 in Galactic coordinates. The approximate size of the young clusters in this region is marked by a dashed circle and labelled. The foreground cluster RCW 36 (0.7 kpc) is located at $l = 265.1$ and $b = 1.4$ and has a reddening $A_V \geq 8$ mag (Ellerbroek et al. 2013); the latter explains the low stellar density in this area. The [KPS2012] MWSC 1594 open cluster is referred to as Cl 1594.

HD 76968 is an O9.2 Ib supergiant that has also been identified as an OB runaway by Carretero-Castrillo et al. (2023) who report a peculiar tangential velocity of 56 km s^{-1}, and we arrive at a similar value of 53 km s^{-1} (Tab. A.3). We do not detect a wind bow shock and obtain a 3D space velocity of 80 km s^{-1} with respect to the LSR and a Z distance of 126 pc below the Galactic plane. Also for this object Bochum 7 could be a potential parent cluster: the kinematical age would then be 4 Myr.

HD 298310 is a B0 V type star with an estimated mass of $\sim 20\,M_\odot$ (Kobulnicky et al. 2019) and a peculiar tangential velocity of about 60 km s^{-1}. Denoyelle (1977) included HD 298310 in their list of young stars with $A_v = 3.71$ mag and obtained a distance of 1.91 kpc in agreement with the *Gaia* distance of $1.9^{+0.04}_{-0.04}$ kpc (Bailer-Jones et al. 2021). The AllWISE colour-composite image of HD 298310 (Fig. 4) shows a bow shock associated with it, although it does not seem to be well aligned with its current motion. The cluster RCW 38 is the likely origin of HD 298310; it moves with a velocity of 52 km s^{-1} with respect to RCW 38 and has escaped from the cluster 3.3 Myr ago.

IRAS 08351-3951 is an M8 type star with a space velocity of 74 km s^{-1}. The AllWISE colour-composite image (Fig. 4) shows an unaligned, not earlier reported arc-like feature close to it. Only in this case, the peak of the arc-like feature emission changes depending on the wavelength range, i.e. the direction from the star to the peak of the 12 μm emission (dashed green arrow) is different from that measured in the 22 μm emission (green arrow). The misaligned bow shock could be explained by large-scale ISM motions (Povich et al. 2008). The path of IRAS 08351-3951 star matches with the IRAS 08337-4028 H II region about 1 Myr ago. IRAS 08337-4028 region contains 39 M-type young stellar objects (Helou & Walker 1988). The age of IRAS 08337-4028 ranges between 1 and 7 Myr (Prisinzano et al. 2018). We identify only 14 members and estimate a cluster age of 0.7–1.0 Myr (Tab. 1). However, the difference in distance of IRAS 08351-3951 ($3.97^{+0.9}_{-0.6}$ kpc) and the IRAS 08337-4028 region ($1.6^{+0.032}_{-0.031}$ kpc) raises suspicions about their connection in the past.

CD-42 4694 is an O9 V type star (Vijapurkar & Drilling 1993) and has a peculiar tangential velocity of 25 km s^{-1}. Denoyelle (1977) included the star in their list of young stars ($A_v = 2.9$ mag) and obtained a distance of 3.5 kpc. The AllWISE colour-composite image (Fig. 4) shows a misaligned bow shock which could be explained by large-scale ISM motions. The constructed path of the star matches with an origin in the PN K 2-15 cluster about 2-3 Myr ago. Massi et al. (2010) identified more than 200 members of the PN K 2-15 cluster and estimated an age of 1-2 Myr. We identify only 12 members and estimate an age of

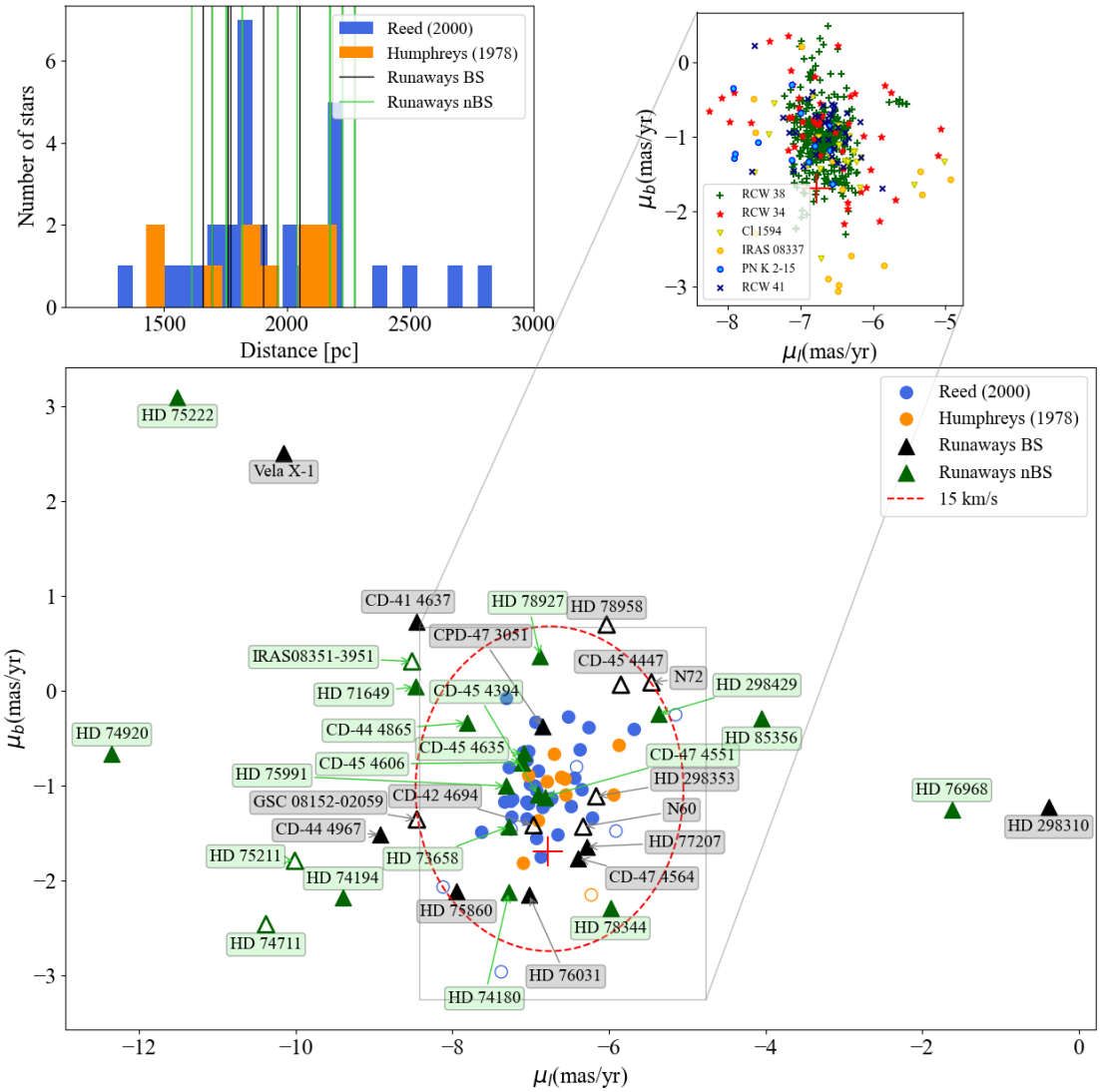

Fig. A.2. *Top-left panel:* The *Gaia* DR3 distance distribution of the candidate members of Vel OB1 (cf. Tab. A.1); candidate members proposed by, respectively, Humphreys (1978) (orange) and Reed (2000) (blue) are indicated. A black vertical line represents the distance to a runaway with an observed bow shock (Runaways BS), and the green vertical lines to those without an observed bow shock (Runaways nBS). *Lower panel:* The *Gaia* DR3 proper motion of the candidate members of Vel OB1 (coloured circles) and runaways (triangles). Runaway stars with and without an associated bow shock are labelled black and green, respectively. Open circles are non-members (see Tab. A.1). Open triangles refer to candidate runaways (see Tab. A.2). The red cross indicates the proper motion of Vel OB1 as reported by Mel'nik & Dambis (2017). The red dashed ellipse indicates a tangential peculiar velocity of 15 km s^{-1} with respect to the mean proper motion of the young massive clusters in Vel OB1. *Top-right panel:* The proper motion distribution of the members of young clusters in Vel OB1. The [KPS2012] MWSC 1594 open cluster and IRAS 08337-4028 are indicated as Cl 1594 and IRAS 08337, respectively.

0.5±3.0 Myr. The age range is in agreement with the kinematical age of CD-42 4694. However, the different distance of the star ($2.47^{+0.15}_{-0.14}$ kpc, Bailer-Jones et al. 2021) compared to that of the PN K 2-15 cluster ($1.79^{+0.023}_{-0.022}$ kpc, Tab. 1) raises suspicions about their connection in the past.

GSC 08152-02059 is an OB type star (Muzzio & Orsatti 1977). The AllWISE colour-composite image (Fig. 4) shows a not earlier reported small arc-like feature very close to it and aligned with its motion (14 km s^{-1}). We have insufficient information to show that this feature is due to a wind bow shock (Sect. 5), and therefore its runaway nature remains to be confirmed. Its path crossed the boundary of RCW 38 about 3–4 Myr ago; its current velocity with respect to RCW 38 is only 4 km s^{-1} which may just be sufficient to have escaped from the cluster (but see 6.4).

DR3 N72 with `source_id` of 5326969910562195072 from *Gaia* DR3 is indicated as N 72 in this work. The AllWISE colour-composite image (Fig. 4) shows an unaligned, not earlier reported arc-like feature close to it. The highest emission of the arc-like feature is not correlated with its symmetry. The arc-like feature remains unaligned even if we take the centre of symmetry. The existence of the unaligned bow shock could be explained by large-scale ISM motions (Povich et al. 2008).

DR3 N60 with `source_id` of 5325934754726652160 from *Gaia* DR3 is indicated as N 60 in this work. Close to it, the AllWISE colour-composite image (Fig. 4) shows an unaligned bow shock-like structure not reported previously, which could be explained by large-scale ISM motions.

Table A.2. Astrometric and kinematic properties of the OB runaway stars in the area of Vel OB1.

Name	l	b	Sp. Type	Parallax	D	μ_{l^*}	μ_b	V_r	V_{pec} 2D (LSR)	V_{pec} 3D (LSR)	(Vel OB1)	Z	Bow shock	Aligned	Angle
–	(deg)	(deg)	–	(mas)	(pc)	(mas yr^{-1})	(mas yr^{-1})	(km s^{-1})	(km s^{-1})	(km s^{-1})	(km s^{-1})	(pc)	–	–	(deg)
(1)	(2)	(3)	(4)	(5)	(6)	(7)	(8)	(9)	(10)	(11)	(12)	(13)	(14)	(15)	(16)
OB runaways with a high peculiar velocity (> 15 km s^{-1}) and/or a bow shock															
HD 71649	255.76	1.00	B1 IIIn	0.442±0.016	2256^{+80}_{-73}	-8.473±0.015	0.045±0.015	–	40	–	37	39	ISM?	–	–
HD 75222	258.29	4.18	B0 Ia	0.494±0.017	2017^{+84}_{-76}	-11.511±0.015	3.096±0.016	64	72	75	*79*	147	N	–	–
CD-41 4637$^{(P)}$	263.02	2.30	O6Ib(f)(n)	0.439±0.013	2280^{+76}_{-62}	-8.456±0.013	0.725±0.013	–	33	–	38	92	Y	Y	30
HD 77581 (Vela X-1)$^{(P)}$	263.06	3.93	B0.5Ia	0.510±0.015	1960^{+57}_{-53}	-10.152±0.015	2.509±0.016	-3.2	51	65	*60*	134	Y	Y	9
HD 74194	264.04	-1.95	O8.5 lb	0.455±0.017	2220^{+125}_{-71}	-9.395±0.020	-2.177±0.019	-2.7	38	54	*51*	-76	N	–	–
HD 75860$^{(P)}$	264.14	0.27	B1.5Iabp	0.450±0.042	2276^{+227}_{-201}	-7.944±0.043	-2.111±0.048	16.8	25	31	*29*	11	Y	Y?	47
HD 76031$^{(P)}$	264.50	0.30	B0.5 IV	0.568±0.025	1752^{+64}_{-63}	-7.024±0.028	-2.147±0.027	–	11	–	6	8	Y	Y	14
HD 73658	264.68	-3.13	B1 II	0.567±0.022	1783^{+86}_{-69}	-7.276±0.023	-1.427±0.023	52	10	23	*26*	-96	N	–	–
CD-44 4865	264.69	-0.37	O9.5 lb	0.514±0.026	1937^{+82}_{-79}	-7.812±0.027	-0.334±0.028	39	14	15	*22*	-13	N	–	–
CD-45 4394	264.87	-2.58	B2 Vne	0.547±0.011	1826^{+37}_{-34}	-6.910±0.012	-1.093±0.013	78	6	46	*53*	-82	N	–	–
HD 74180	265.28	-2.95	F2 Ia	0.440±0.101	2532^{+600}_{-397}	-7.277±0.107	-2.118±0.122	31	23	22	*26*	-117	N	–	–
HD 74920	265.29	-1.95	O7.5IVn((f))	0.574±0.026	1753^{+63}_{-68}	-12.351±0.029	-0.661±0.032	–	50	–	45	-60	N	–	–
CD-45 4606	265.44	-0.94	B0.5 V	0.463±0.012	2149^{+57}_{-60}	-7.109±0.012	-0.752±0.014	6	9	30	*24*	-35	N	–	–
CD-45 4635	265.67	-0.90	B0.5 III	0.449±0.014	2235^{+65}_{-67}	-7.090±0.015	-0.657±0.016	18	9	19	*18*	-35	N	–	–
CD-44 4967	266.01	0.00	OB+	0.603±0.010	1663^{+30}_{-25}	-8.819±0.012	-2.031±0.013	–	20	–	12	0.1	Y	Y	11
HD 78927	266.02	3.10	B1 II/III	0.464±0.020	2169^{+76}_{-67}	-6.879±0.020	0.365±0.022	27	16	17	*21*	117	ISM?	–	–
HD 75991	267.17	-2.07	B0.5 III	0.619±0.015	1618^{+39}_{-39}	-7.313±0.016	-1.002±0.016	9	5	20	*15*	-58	N	–	–
CD-47 4551	267.98	-1.36	O5 Ifc	0.588±0.028	1697^{+95}_{-75}	-6.816±0.032	-1.115±0.033	136	2	107	*114*	-40	ISM	N	177
CD-47 4564	268.46	-1.65	B0.5 III	0.574±0.017	1718^{+44}_{-52}	-6.393±0.019	-1.761±0.020	-2	8	31	*25*	-49	Y	Y?	56
HD 78344	268.89	-0.38	O9.5/B0 (Ib)	0.452±0.016	2169^{+82}_{-83}	-5.982±0.017	-2.286±0.016	-5.7	17	42	*29*	-14	N	–	–
HD 77207	268.96	-1.90	B7Iab+	0.564±0.017	1784^{+40}_{-50}	-6.292±0.018	-1.638±0.017	–	8	–	7	-59	Y	Y?	68
CPD-47 3051	269.21	-0.91	B0V	0.487±0.019	2069^{+70}_{-77}	-6.856±0.021	-0.372±0.021	–	4	–	12	-33	Y	Y	9
HD 76968	270.22	-3.37	O9.2Ib	0.455±0.019	2199^{+97}_{-83}	-1.619±0.022	-1.247±0.021	-22	53	74	*61*	-129	N	–	–
HD 298310	272.58	-1.72	B0V	0.525±0.011	1900^{+37}_{-35}	-0.468±0.012	-1.088±0.013	-27	59	80	*72*	-57	Y	N	126
HD 85356	274.37	4.60	B2Ib	0.571±0.034	1754^{+103}_{-96}	-4.049±0.036	-0.288±0.033	–	27	–	28	141	N	–	–
HD 298429	274.47	-0.25	O8.5 V	0.548±0.011	1831^{+46}_{-44}	-5.369±0.013	0.245±0.013	25	18	20	*23*	-8	N	–	–
Candidate OB runaways in the field centered on Vel OB1															
IRAS 08351-3951	259.62	0.55	M8	0.272±0.050	3975^{+916}_{-590}	3.736±0.050	7.659±0.055	35	71	74	*94*	38	ISM	N	90
CD-42 4694	263.61	0.55	O9V	0.409±0.027	2466^{+148}_{-137}	-6.966±0.027	-1.413±0.028	–	13	–	22	24	Y?	N	145
HD 75211	263.96	-0.47	O9 Ib	0.633±0.015	1550^{+31}_{-36}	-10.013±0.016	-1.789±0.015	20	27	30	*17*	-13	N	–	–
CD-45 4447	265.18	-2.26	O7.5 V	1.528±0.394	888^{+337}_{-221}	-5.848±0.449	0.066±0.451	–	11	–	42	-26	Y?	Y?	67
HD 74711	265.73	-2.61	B1 III	0.785±0.022	1272^{+37}_{-35}	-10.381±0.023	-2.458±0.025	–	23	–	5	-58	N	–	–
GSC 08152-02059	265.88	-0.39	OB	0.668±0.018	1507^{+43}_{-40}	-8.453±0.019	-1.354±0.022	–	14	–	3	-10	Y?	Y?	65
HD 78958	266.47	2.73	B0/1 Iab	0.469±0.012	2133^{+54}_{-39}	-6.030±0.011	-0.700±0.012	35	4	5	*14*	101	Y?	N	132
DR3 N72	269.01	-0.76	–	0.336±0.035	2927^{+615}_{-242}	-5.457±0.040	0.090±0.040	42	11	12	*30*	-39	Y?	N	112
DR3 N60	270.91	-0.73	–	0.419±0.039	2410^{+245}_{-155}	-6.329±0.046	-1.430±0.042	–	10	–	15	-31	Y	N	119
HD 298353	273.12	-1.96	O7V	0.377±0.012	2680^{+89}_{-82}	-6.163±0.015	-1.110±0.015	–	9	–	21	-92	Y	N	93

Notes. (1) name of star, (2), (3) Galactic coordinates of star, (4) spectral type, (5) *Gaia* DR3 corrected parallax and parallax uncertainty, (6) distance estimated by Bailer-Jones et al. (2021) with uncertainty, (7) (8) *Gaia* DR3 galactic proper motion and proper motion uncertainty, (9) radial velocity, (10) and (11) transverse and peculiar velocity relative to LSR, respectively, (12) transverse or peculiar (*italic*)) velocity relative to Vel OB1, (13) distance from the Galactic plane, (14) observed bow shock, (15) alignment status of observed bow shock, and (16) mis-alignment angle. Two objects are indicated as DR3 N72 and N60 based on their last numbers of `source_id` from *Gaia* DR3. Objects in common with Carretero-Castrillo et al. (2023) are in bold. (P) - objects included in Patten et al. (2025).

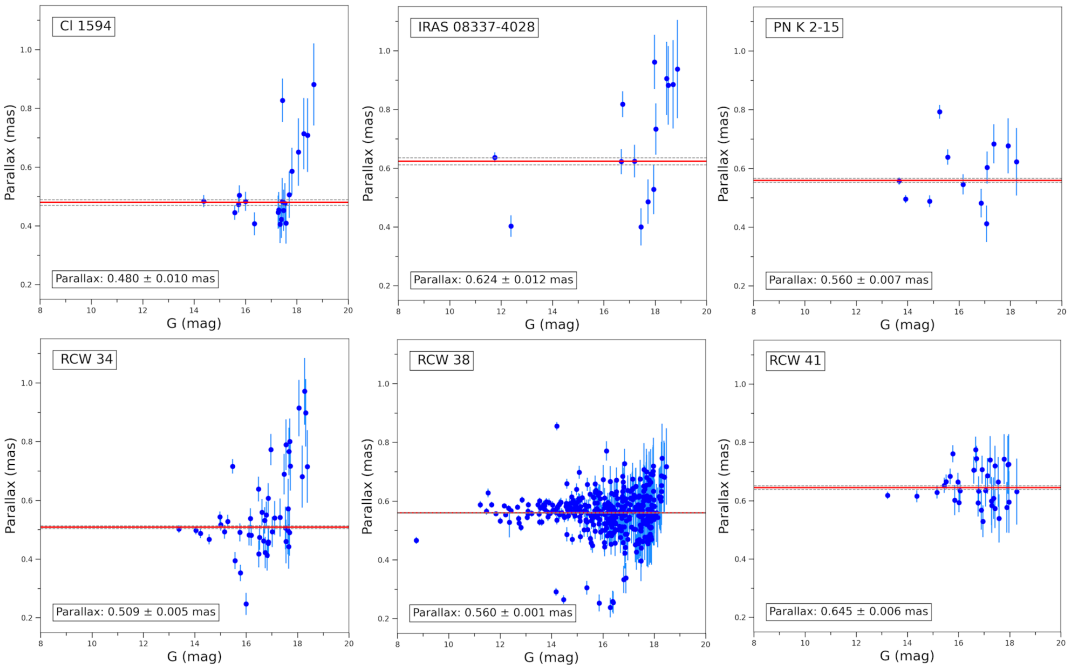

Fig. B.1. Parallax distribution as a function of the G-magnitude for each stellar cluster. The best-fit parallax and 1σ uncertainty for the cluster members are shown with the red and grey lines, respectively. The [KPS2012] MWSC 1594 open cluster is indicated as Cl 1594.

Table A.3. Estimate of the kinematical age of the OB runaways in Vel OB1.

Name	l	b	D	V_r	V_{pecLSR}	Runaway direction	Age_{kinGP}	Parent	D_{par}	Age_{kinpar}	V_{pecpar}
–	(deg)	(deg)	(pc)	(km s^{-1})	(km s^{-1})	–	(Myr)	–	(pc)	(Myr)	(km s^{-1})
(1)	(2)	(3)	(4)	(5)	(6)	(7)	(8)	(9)	(10)	(11)	(12)
HD 75222	258.29	4.18	2017^{+84}_{-76}	64	72/**75**	A	4.9; 3.7; 2.5	Bochum 7	2245*	5.5	**67**
CD-41 4637	263.02	2.30	2280^{+76}_{-62}	–	33	A?	11; 6.5; 1.5	RCW 34	$1967^{+18.4}_{-18.0}$	2	35
GSC 08152-02059	265.88	-0.39	1507^{+43}_{-40}	–	14	A	1.0; –; –	RCW 38	$1785^{+4.2}_{-4.1}$	3-4	4
HD 76968	270.22	-3.37	2199^{+97}_{-83}	-22	53/**74**	A?	9.7; 6.8; 4.0	Bochum 7	2245*	4	**75**
HD 298310	272.58	-1.72	1900^{+37}_{-35}	-27	59/**80**	A	5.7; 2.4; –	RCW 38	$1785^{+4.2}_{-4.1}$	3.3	52
HD 71649	255.76	1.00	2256^{+80}_{-73}	–	40	P	–	–	–	–	–
HD 77581 (Vela X-1)	263.06	3.93	1960^{+57}_{-53}	-3.2	51/**65**	A	5.6; 4.2; 2.8	Vel OB1/RCW 38?	$1785^{+4.2}_{-4.1}$	2.3/4-5	**60**/53
HD 74194	264.04	-1.95	2220^{+125}_{-73}	-2.7	38/**54**	A	3.2; 1.6; –	[FSR2007]1452	2549*	4	**35**
HD 75860	264.14	0.27	2276^{+227}_{-201}	16.8	25/**31**	T	–	Cl 1594?	$2084^{+43.0}_{-41.3}$	1.2	24
HD 76031	264.50	0.30	1752^{+64}_{-63}	–	11	T	–	–	–	–	–
HD 73658	264.68	-3.13	1783^{+86}_{-66}	52	10/**23**	A?	7.9; 5.4; 2.9	–	–	–	–
CD-44 4865	264.69	-0.37	1937^{+82}_{-79}	39	14/**15**	P	–	–	–	–	–
CD-45 4394	264.87	-2.58	1826^{+37}_{-34}	78	6/**46**	A?	8.5; 5.2; 1.9	–	–	–	–
HD 74180	265.28	-2.95	2532^{+600}_{-397}	31	23/**22**	A	5.0; 3.3; 1.6	–	–	–	–
HD 74920	265.29	-1.95	1753^{+63}_{-68}	–	50	P	–	Cluster?	2020^{+13}_{-12}	0.2-0.3	38
CD-45 4606	265.44	-0.94	2149^{+97}_{-60}	6	9/**30**	P?	–	–	–	–	–
CD-45 4635	265.67	-0.90	2235^{+165}_{-67}	18	9/**19**	P?	–	–	–	–	–
CD-44 4967	266.01	0.00	1663^{+30}_{-25}	–	20	T	–	RCW 38?	$1785^{+4.2}_{-4.1}$	3-4	16
HD 78927	266.02	3.10	2169^{+76}_{-87}	27	16/**17**	P	–	–	–	–	–
HD 75991	267.17	-2.07	1618^{+39}_{-39}	9	5/**20**	A?	7.4; 3.8; 0.3	–	–	–	–
CD-47 4551	267.98	-1.36	1697^{+95}_{-75}	136	2/**107**	A	4.4; 1.2; –	–	–	–	–
CD-47 4564	268.46	-1.65	1718^{+44}_{-52}	-2	8/**31**	A	3.4; 1.3; –	–	–	–	–
HD 78344	268.89	-0.38	2169^{+82}_{-83}	-5.7	17/**42**	A	0.6; –; –	–	–	–	–
HD 77207	268.96	-1.90	1784^{+40}_{-50}	–	8	A	4.2; 2.0; –	–	–	–	–
CPD-47 3051	269.21	-0.91	2069^{+70}_{-77}	–	4	P	–	–	–	–	–
HD 85356	274.37	4.60	1754^{+103}_{-96}	–	27	P	–	–	–	–	–
HD 298429	274.47	-0.25	1831^{+46}_{-44}	25	18/**20**	P	–	–	–	–	–
IRAS 08351-3951	259.62	0.55	3975^{+916}_{-599}	35	71/**74**	T	–	IRAS 08337-4028?	$1603^{+31.7}_{-30.5}$	1	109
CD-42 4694	263.61	0.55	2466^{+188}_{-137}	–	13	T	–	PN K 2-15?	$1787^{+23.0}_{-22.4}$	2-3	25
HD 75211	263.96	-0.47	1550^{+31}_{-36}	20	27/**30**	A	0.9; –; –	Muzzio 1	1797*	4	122
CD-45 4447	265.18	-2.26	888^{+337}_{-221}	–	11	P	–	–	–	–	–
HD 74711	265.73	-2.61	1272^{+37}_{-35}	–	23	A	3.8; 2.4; 0.9	–	–	–	–
HD 78958	266.47	2.73	2133^{+54}_{-39}	35	4/**5**	P	–	–	–	–	–
DR3 N72	269.01	-0.76	2927^{+605}_{-242}	42	11/**12**	P	–	–	–	–	–
DR3 N60	270.91	-0.73	2410^{+245}_{-155}	–	10	A	1.8; –; –	–	–	–	–
HD 298353	273.12	-1.96	2680^{+89}_{-82}	–	9	A?	6.4; 3.1; –	–	–	–	–

Notes. (1) Name of the OB runaway; (2) and (3) Galactic coordinates; (4) Distance with uncertainty (Bailer-Jones et al. (2021)); (5) Radial velocity; (6) Transverse/ peculiar velocity (thus including radial velocity in *bold*) relative to the LSR; (7) Direction of the runaway: A – away from the Galactic plane, P – parallel to the Galactic plane, T – toward the Galactic plane; (8) Kinematic age assuming that the OB runaway originates at b=0°, b=1°, or b=2°, respectively; (9) Parent cluster; (10) Distance of the parent cluster, (11) Kinematic age if ejected from the proposed parent cluster; and (12) Peculiar transverse velocity of the star relative to its origin, and when the radial velocity is included (*bold*). The [KPS2012] MWSC 1594 open cluster is indicated as Cl 1594. The ID of DR3 N72 and N60 is based on their last numbers of `source_id` from *Gaia* DR3. Objects in common with Carretero-Castrillo et al. (2023) are in bold. (*) The distances of these clusters are taken from Cantat-Gaudin & Anders (2020); Poggio et al. (2021); Tarricq et al. (2021).

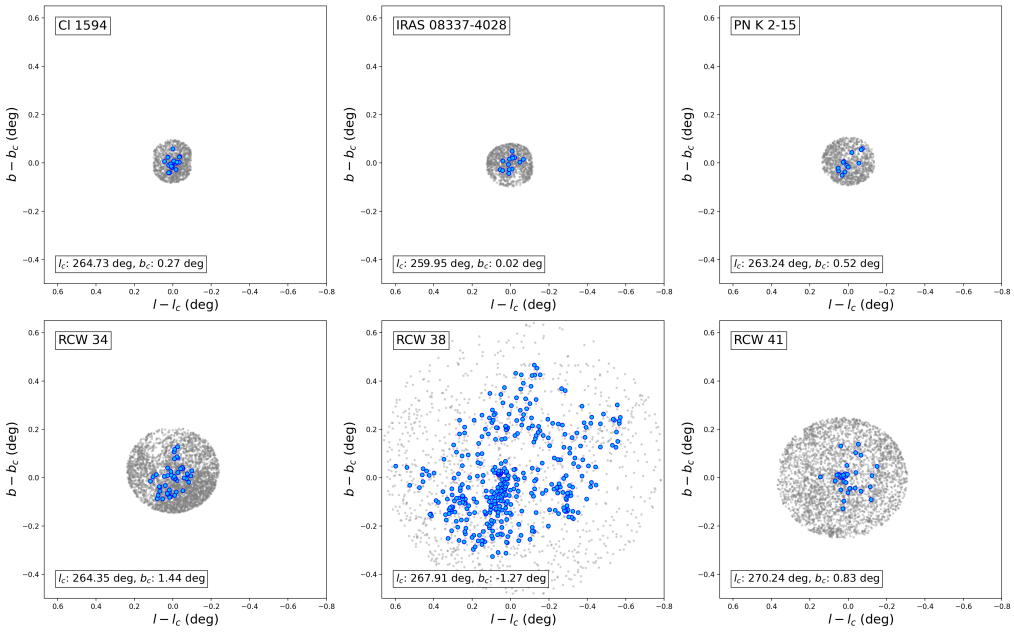

Fig. B.2. Distribution of members for each stellar cluster with field stars. Members and field stars are in blue and grey, respectively. The median value of the cluster coordinates is taken as the centre of each panel. Visual inspection of the image of RCW 38 shows that the extinction is low where the members show high density which we called "condensation". The [KPS2012] MWSC 1594 open cluster is indicated as Cl 1594.

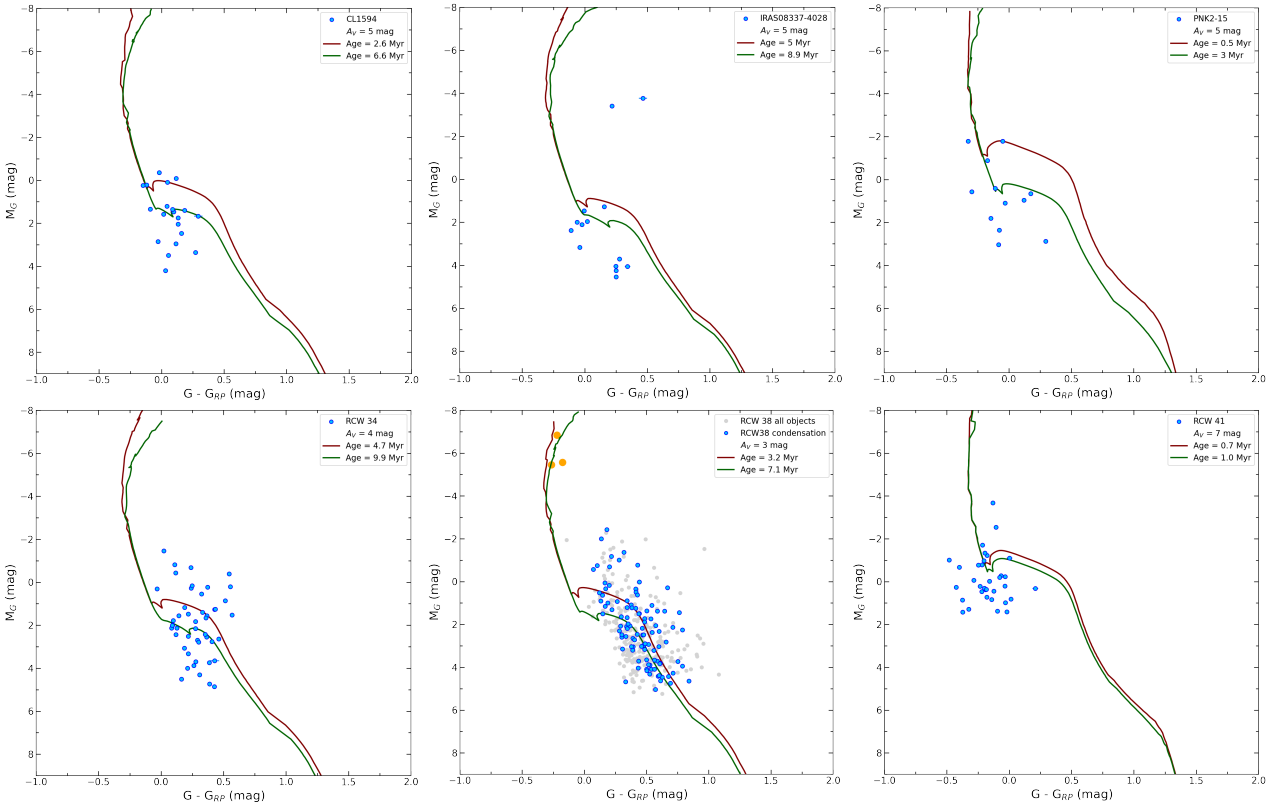

Fig. B.3. Colour-absolute magnitude diagrams for members of each parent cluster. The members are blue dots. In RCW 38 the fitting is carried out for objects with similar A_v (blue dots) named "condensation" (see Fig. B.2) not with all members (grey dots). The upper and lower age isochrones are based on 100 iterations and are represented by the red and green curves, respectively. Orange circles are OB-star members of RCW 38 (see Tab. A.1). Absolute magnitudes are determined from individual parallaxes. The [KPS2012] MWSC 1594 open cluster is indicated as Cl 1594.

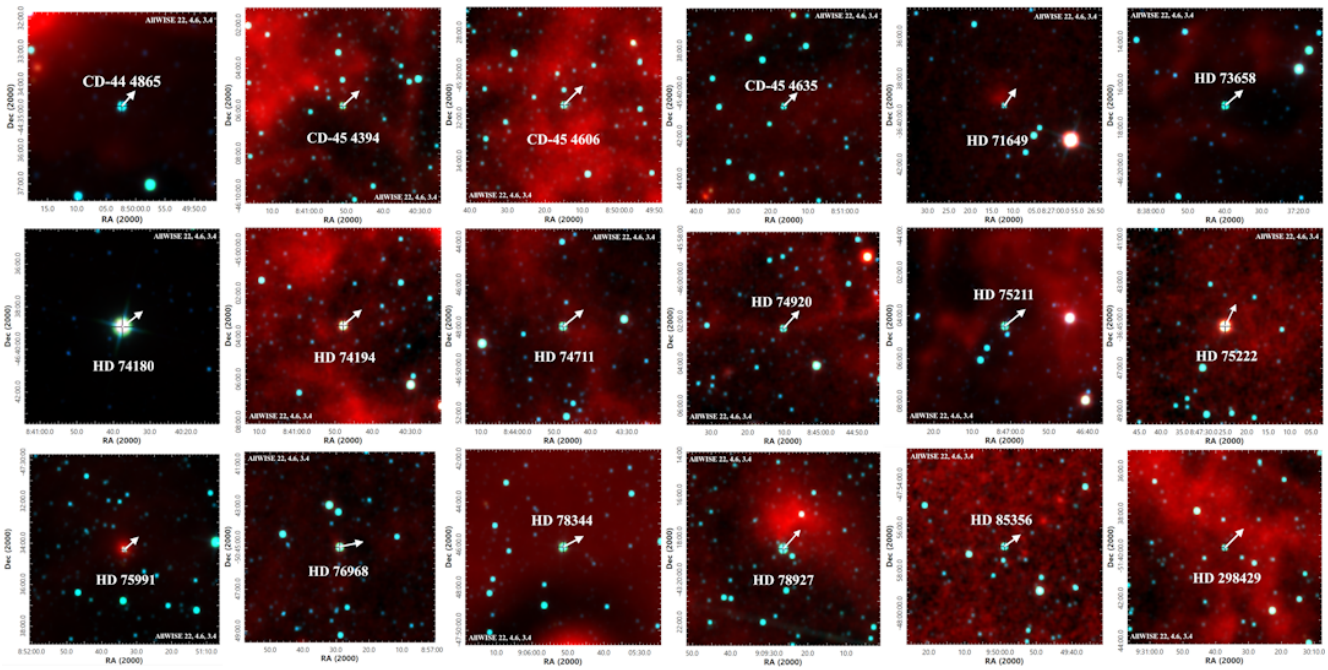

Fig. C.1. AllWISE colour-composite images of runaway stars with high peculiar velocity in the Vel OB1 association. The runaway stars are marked with a cross. The white arrow indicates the direction of current proper motion of each star.